NAVAL POSTGRADUATE SCHOOL
Monterey, California

THESIS

CALCULATING TROPICAL CYCLONE CRITICAL WIND RADII AND STORM SIZE USING NSCAT WINDS

by

Scott G. Magnan

March, 1998

Thesis Advisor: Russell L. Elsberry
Thesis Co-Advisor: Lester E. Carr, III

REPORT DOCUMENTATION PAGE

Form Approved OMB No. 0704-0188

1. AGENCY USE ONLY *(Leave blank)*	2. REPORT DATE March, 1998.	3. REPORT TYPE AND DATES COVERED Master's Thesis

4. TITLE AND SUBTITLE CALCULATING TROPICAL CYCLONE CRITICAL WIND RADII AND STORM SIZE USING NSCAT WINDS	5. FUNDING NUMBERS
6. AUTHOR(S) Scott G. Magnan	

7. PERFORMING ORGANIZATION NAME(S) AND ADDRESS(ES) Naval Postgraduate School Monterey CA 93943-5000	8. PERFORMING ORGANIZATION REPORT NUMBER

9. SPONSORING/MONITORING AGENCY NAME(S) AND ADDRESS(ES)	10. SPONSORING/MONITORING AGENCY REPORT NUMBER

11. SUPPLEMENTARY NOTES The views expressed in this thesis are those of the author and do not reflect the official policy or position of the Department of Defense or the U.S. Government.

12a. DISTRIBUTION/AVAILABILITY STATEMENT Approved for public release; distribution is unlimited.	12b. DISTRIBUTION CODE

13. ABSTRACT *(maximum 200 words)*

Subjective and objective analyses of satellite scatterometer near-surface winds are utilized to estimate tropical cyclone (TC) critical wind radii and size over a region of the western North Pacific. An outer wind profile assuming a linear slope dependent on the TC latitude is used to determine the radial extent of cyclonic winds beyond a set radius. Inside the set radius, a partial conservation of angular momentum is assumed into the TC maximum wind radius and the 35-, 50-, and 100-kt radii are calculated. Nine TCs were investigated during the operating period of the NASA scatterometer (NSCAT). Critical wind radii values in four quadrants (front, right, rear, and left) of the TCs are found to be comparable to the Joint Typhoon Warning Center (JTWC) critical wind radii values issued in warnings. The radial extent of cyclonic winds are also comparable to the radius of zero winds estimated by determining where the cyclonic flow turned to anticyclonic flow in the NSCAT sea-surface wind swaths.

14. SUBJECT TERMS Tropical cyclone wind structure, NASA scatterometer, Tropical cyclonic size	15. NUMBER OF PAGES 69
	16. PRICE CODE

17. SECURITY CLASSIFICATION OF REPORT Unclassified	18. SECURITY CLASSIFICATION OF THIS PAGE Unclassified	19. SECURITY CLASSIFICATION OF ABSTRACT Unclassified	20. LIMITATION OF ABSTRACT UL

NSN 7540-01-280-5500

Standard Form 298 (Rev. 2-89)
Prescribed by ANSI Std. 239-18 298-102

DTIC QUALITY INSPECTED 3

CALCULATING TROPICAL CYCLONE CRITICAL WIND RADII AND STORM SIZE USING NSCAT WINDS

Scott G. Magnan
Captain, United States Air Force
B.S., State University of New York, Oneonta, 1990

Submitted in partial fulfillment
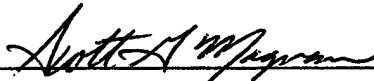of the requirements for the degree of

MASTER OF SCIENCE IN METEOROLOGY

from the
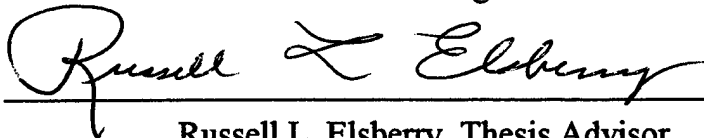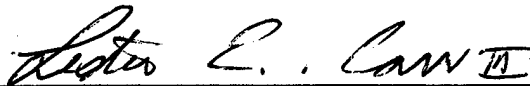
NAVAL POSTGRADUATE SCHOOL
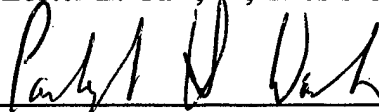**March 1998**

Author: _____
Scott G. Magnan

Approved by: _____
Russell L. Elsberry, Thesis Advisor

_____
Lester E. Carr, III, Thesis Co-Advisor

_____
Carlyle H. Wash, Chairman
Department of Meteorology

iii

iv

ABSTRACT

Subjective and objective analyses of satellite scatterometer near-surface winds are utilized to estimate tropical cyclone (TC) critical wind radii and size over a region of the western North Pacific. An outer wind profile assuming a linear slope dependent on the TC latitude is used to determine the radial extent of cyclonic winds beyond a set radius. Inside the set radius, a partial conservation of angular momentum is assumed into the TC maximum wind radius and the 35-, 50-, and 100-kt radii are calculated. Nine TCs were investigated during the operating period of the NASA scatterometer (NSCAT). Critical wind radii values in four quadrants (front, right, rear, and left) of the TCs are found to be comparable to the Joint Typhoon Warning Center (JTWC) critical wind radii values issued in warnings. The radial extent of cyclonic winds are also comparable to the radius of zero winds estimated by determining where the cyclonic flow turned to anticyclonic flow in the NSCAT sea-surface wind swaths.

TABLE OF CONTENTS

ACKNOWLEDGMENTS

This research would not have been possible without the outstanding support from several people at the Naval Postgraduate School. Mr. Mark Boothe created and assisted with numerous computer programs, as well as graphic representation of the output. Ms. Mary Jordan assisted with the code for reading and plotting large amounts of data. I also want to thank my co-advisor Professor Les E. Carr, III for his expertise and assistance in the application of his tropical cyclone wind distribution model. Foremostly, I want to thank my advisor Professor Russ Elsberry for the expert guidance and patience he provided over the many paths taken to reach the final results.

x

I. INTRODUCTION

A. BACKGROUND

Setting of critical wind warnings and beginning of various disaster preparedness activities are essential to minimize loss of lives and property owing to potential high winds, excessive rainfall, and storm surge in the Tropical Cyclone (TC). The timing of the warnings depends on the distance to the TC center, translation speed, and the wind structure in the TC vortex. For example, a threshold such as gale-force wind will be surpassed earlier for a large TC than for a midget TC if the TCs are following the same track.

Before the onset of damaging winds, the civilian population needs to secure and protect personal property, prepare for evacuation from low-lying areas, set up emergency shelters, and assemble rescue teams. The military forces need to reroute ships at sea, evacuate aircraft from air bases, as well as accomplish the tasks performed by the civilian population. In the western North Pacific, a TC Selective Reconnaissance Program (SRP) is set up to track and analyze TCs using meteorological satellites. Four stations have Defense Meteorological Satellite Program (DMSP), National Oceanic and Atmospheric Administration (NOAA), and geostationary satellite imagery receiving capabilities. The Joint Typhoon Warning Center (JTWC) at Nimitz Hill on Guam monitors the SRP network and analyzes TCs using primarily the Japanese Geostationary Meteorological Satellite (GMS-5); Kadena AB on Okinawa, Japan, provides the JTWC with TC analyses using polar-orbiting DMSP and NOAA satellite imagery ingested via the MARKIVB Meteorological Data Station (MDS); Osan AB in Korea provides analyses using polar-orbiting satellite imagery from the MARKIV van; and Hickam AFB in Hawaii also utilizes the MARKIVB MDS to provide TC

1

fixes to the JTWC.

The network centers perform a Dvorak position and intensity analysis on each satellite image with good coverage of the TC. The analysis includes determining the TC vorticity center by inferring it from various cloud patterns, with the easiest being the well- defined eye of the TC, if one exists. The second part of the analysis involves estimating the TC intensity by measuring various cloud features (size and/or temperature), pattern recognition, or using the previous reports to aid in determining what the TC intensity should be if it is in an intensifying, weakening, or steady state. The intensities provide only an estimate of the maximum wind speed found near the center of the TCs and give no information about the TC outer wind structure, e.g., how far from the center of the TC the 35-kt winds are found.

The JTWC is responsible for using these position/intensity reports to aid them in determining the TC forecast track and extent of critical wind radii for TCs located west of 180° longitude to the east coast of Africa, north and south of the equator. Military operations in the western North Pacific are based on these TC warnings. The Typhoon Duty Officer (TDO) works in close proximity to the office responsible for routing ship traffic in the Pacific. Other military bases receive the TC warning via the Automated Weather Network (AWN). Once received, the base weather station takes immediate action by determining the onset of critical winds. The wind direction as well as the speed is important to flight operations for determining if and/or when runway cross-wind limitations will be exceeded. The base commander needs accurate timing to put aircrews into crewrest so that a timely evacuation of aircraft may be accomplished from a threatened air base, and then missions may continue from other staging bases. When commanders evacuate aircraft unnecessarily, or

2

excessive runway cross-winds occur sooner than forecast, credibility of the weather forecaster begins to dwindle. The military population on Okinawa is alerted to the threat via a Tropical Cyclone Condition Of Readiness (TCCOR), which is set by the senior military commander based on the JTWC TC warnings and expected local surface wind conditions as interpreted by the base weather station. The TCCOR numbers are: 4, onset of 50-kt winds is possible within 72 h; 3, 50-kt winds are possible within 48 h; 2, 50-kt winds are expected within 24 h; and 1, 50-kt winds are expected within 12 h. Special conditions within TCCOR = 1 are also defined: 1C, 35-kt winds occurring, 50-kt expected soon, no one allowed outside; 1E, 50-kt winds occurring; 1R, 35-kt winds occurring, 50-kt winds no longer expected, recovery personnel allowed outside; and All Clear, damaging winds no longer expected. The TC wind structure as well as the track inputs determine the TCCOR timing. The Kadena AB weather station is responsible for providing the wind information to the wing commander, who is responsible for setting the TCCOR for all military activities on Okinawa (30,000 active duty personnel most with families).

Once the TCCOR is set, the weather station conducts a conference call with other base points of contact. Those contacts disseminate the TCCOR through their chain of command. The Kadena weather station provides a person to the Armed Forces Radio and Television Service when TCCORs are set. This person provides live updates of the TCCOR. The weather station also has the ability to provide and update an emergency banner message across the bottom of the television screen through the Americable television company on Okinawa. The weather station updates, on a six-hour basis, the automated telephone answering system that solely provides TCCOR information (the automated telephone receives

approximately 1,400 calls a day during low TCCORs).

B.   TROPICAL CYCLONE WIND STRUCTURE

TC intensity is defined as the maximum estimated surface winds in the storm, which are usually located near the edge of the eye wall cloud. Riehl (1963) found that the tangential wind at a height near the surface inflow layer (approximately 3,000 ft) radial profile could be represented as $v_\theta r^x$=constant with a x coefficient of 0.5. Riehl suggested this validated the principle of conservation of potential vorticity and concluded that hurricanes could not be regarded as fully isolated vortices and that they may be influenced strongly by external circulation. Holland (1980) modified the Schloemer (1956) profile by allowing for adjustment of the sharpness of the wind profile to fit the range of shapes found in nature, and these modified profiles have been used with some success in extrapolating inward from observations at larger radii. Merrill (1984) noted the importance of distinguishing between the "intensity" of the cyclone core and the "strength" of the outer circulation. Weatherford and Gray (1988a,b) confirmed the low correlation between strength and intensity using reconnaissance aircraft data from the western North Pacific.

For this paper, the definition of TC size is the outer limit of cyclonic wind, or where the wind changes from cyclonic to anticyclonic. The first definition of the size of the TC is implied in a wind profile proposed by Carr and Elsberry (1994, 1997). They define a radial extent of the cyclonic tangential winds (R_0) that may be thought of as a size specification. The strength of the TC will be viewed as the area under the tangential wind radial profile at some outer radius.

The analysis of critical wind radii at the JTWC is hindered by inadequate data.

Monitoring of the TC wind structure is based on observations such as low-level cloud-drift winds from geostationary satellite visible and infrared instrumentation, a few rawinsonde soundings, ship and shore station reports, and radar observations. Analyses of such observations of the low-level wind structure in TCs are required for improved TC warnings of critical threshold wind values, such as the 35-kt and 50-kt wind radii. This TC size determination is important to the warning process throughout the TC life cycle, and is particularly important for accurate forecasts of onset winds in the 0-36 h time frame.

A size estimate is also important for understanding whether significant deviations of the motion from the steering current will be expected. Improved synthetic wind observations in dynamical track prediction models, improved ocean forcing estimates, and understanding of the relationships between the TC vortex and the environment during formation and throughout the life cycle are imperative to enhance current prediction techniques.

Fisher (1996) computed R_0^{850} for 165 western North Pacific storms and found that for about 40% of the storms R_0 did not increase after the intensity reached a value in the range of 50-60 kt. The remaining 60% of the TCs demonstrated growth in R_0^{850} throughout the intensification phase. Of those 40% of the cases in which R_0 did not continue to grow throughout the intensification phase, about 60% had a contracting R_0 with an increase in intensity and about 40% had a relatively constant R_0 with an increase in intensity. Fisher found the range of TC intensities at which the majority of the R_0 trend change occurs is between 41-70 kt. The majority of the TCs that had a change in R_0 trend at higher intensities tended to then have a decrease in R_0 during the remainder of the intensification phase.

Carr and Elsberry (1994, 1997) proposed a tangential wind profile model for

5

estimating R_0^{850} (radius of zero cyclonic wind at 850 mb) for subsequent tropical cyclone size estimates. This model is based on partial conservation of absolute angular momentum, and thus best applies at outer wind radii where the frictional losses of momentum are not as large. The Carr and Elsberry wind profile relationship is

$$V = \frac{M}{r^x} - \frac{1}{2} f_0 r,$$

where

$$M = \frac{1}{2} f_0 R_0^{1+x}.$$

Here, V is the tangential wind velocity at the 850 mb level, r is the radius from the center, R_0 is the radius of zero cyclonic wind, f_0 is the Coriolis parameter at the latitude of the tropical storm, and M is the angular momentum at the radius R_0. A complete derivation of these equations is provided in Carr and Elsberry (1997). The value of the "x" exponent is set to 0.4 when these equations are used for wind profiles in the low troposphere above the boundary layer. Carr and Elsberry demonstrate that the exponent value of x=0.4 is reasonably accurate at various radii in the TC and is in approximate agreement with observed TC tangential wind profiles. They also illustrate the differences in the tangential wind profiles as the exponent "x" is varied from 0.3 to 0.5. As these differences are mainly found within 300 km of the TC center, they have almost no effect on the beta-effect propagation speed, which depends on the outer wind structure. Carr and Elsberry inserted initially symmetric vortices with various angular momentum profiles into a nondivergent, barotropic model and found significantly

different beta-effect propagation speeds.

Meteorological satellites provide new sources of wind structure over the earth's oceans. Recent DMSP satellites are equipped with the Special Sensor Microwave Imager (SSM/I) that provides wind speed only (passive microwave techniques). The SSM/I measures ocean surface backscatter to determine the wind speed. The higher the wind speed, the rougher the ocean surface, and the greater the backscatter. The sensor accuracy is limited by rain contamination that "smoothes" the surface seas, decreases the amount of backscatter, and results in a lower wind speed estimate. The swath of data is approximately 800 nautical miles wide. The algorithm used to determine wind speed can resolve speeds up to 50 kt. However, no process is available for determining wind direction.

Scatterometers are currently the main source for ocean surface wind vectors. In contrast to SSM/I, scatterometers (active microwave instruments) have the ability to provide wind direction and magnitude. Scatterometers also operate by recording the change in radar reflectivity of the sea due to the generation of small ripples on the ocean surface by the wind. The Earth Remote-sensing Satellites (ERS) 1 and 2 operated by the European Space Agency (ESA) provide a single 500 km wide swath of ocean wind data. The wind direction accuracy is $+\text{-}20°$ within a wind speed range of 4 m s^{-1}- 24 m s^{-1}, and wind speed accuracy of 2 m s^{-1} or 10%. JTWC uses ERS scatterometer data when available to determine the R_{35} value of storms. The ERS swath is displayed as colored wind barbs so that the 35-kt wind radii is immediately evident. However, an adjustment is made to the ERS wind speed because it has been found the ERS wind speeds are lower than ship report speeds. The result is the R_{35} distance is larger than is displayed by the colored wind barbs along the data swath.

The NASA Scatterometer (NSCAT) managed for NASA by the Jet Propulsion Laboratory was successfully launched 16 August 1996. The NSCAT was the first dual-swath scatterometer since SEASAT in 1978. The dual-swath capability returned two 600 km wide swaths of ocean wind speed and direction. The failure of Japan's Advanced Earth Observing Satellite (ADEOS) with the NSCAT aboard resulted in the loss of the scatterometry data on 30 June 1997.

C.   PURPOSES OF THESIS

One objective of this research is to combine scatterometer data with the satellite techniques for observing TCs to provide a more objective analysis of TC wind structure to aid Typhoon Duty Officers (TDOs) in the preparation of TC warnings. Another objective is to describe the characteristics of western North Pacific TCs during the NSCAT operational time period.

II. SCATTEROMETRY

A.   PRINCIPLES

Spaceborne scatterometers transmit microwave pulses to the ocean surface and measure the backscattered power received at the instrument. Wind velocity changes create changes in the sea-surface roughness, which modifies the radar cross section, and therefore the magnitude of the backscattered power. Scatterometers measure the backscattered power, which allows estimation of the normalized radar cross section (σ_0). An empirical relationship between radar cross section and near-surface winds enables the extraction of wind velocity from backscatter measurements. The radar equation is used to calculate the σ_0 after the instrument noise power is estimated and subtracted from the total power received.

The geophysical model function is the relationship between the σ_0 and the near-surface wind. The model function may not be derived from theory alone due to the lack of understanding of both the relationship between the wind and the sea-surface roughness, and the interaction between the electromagnetic radiation and the sea surface. Backscattered radiation results primarily from resonant Bragg scattering from short ocean waves with wavelengths comparable to that of the incident electromagnetic radiation (approximately 2 cm). In addition, σ_0 is a sensitive function of wind direction (χ) as measured relative to the radar azimuth angle (Fig. 2.1; figures are at end of chapter). The relationship between the σ_0 and azimuth angle is nearly $\cos(2\chi)$, with the σ_0 having maxima at upwind ($\chi=0°$) and downwind ($\chi=180°$) angles, and minima near crosswind ($\chi=90°$ and $270°$) angles (Fig. 2.2). Upwind cross section values are usually larger than downwind, which is known as the

9

upwind-downwind asymmetry. This small asymmetry is critical because it makes possible scatterometer vector wind measurements to determine if the wind was blowing "from" or "to" a given direction (180° ambiguity in direction).

Estimation of wind velocity from a σ_0 measurement involves inversion of the geophysical model function. Multiple σ_0 measurements need to be made to arrive at a unique wind vector solution. With two antennas set apart 90° (same polarity), up to four possible solutions will be derived (Fig. 2.3). With the addition of another dual-polarized antenna at an angle between these two, the number of solutions is reduced to one.

B.   APPLICATION TO NSCAT

The NSCAT, which was a spaceborne microwave radar scatterometer, measured near-surface (10 m) wind vectors (both speed and direction) over the global oceans from September 1996 to June 1997. The NSCAT was launched aboard the Advanced Earth Observing Satellite (ADEOS), which was a mission of the National Space Development Agency (NASDA) of Japan.

NSCAT had six stick-type antennas that generated fan beam footprints on the ocean surface. The mid-beams were dual-polarized, which allowed for a total of eight independent antenna/polarization combinations (Fig. 2.4). The antenna swept a 600 km swath on each side with a 350-400 km gap between the two swaths. The right-side antennas are numbered 1-3: Antenna 1 is set at 45° with vertical polarization; Antenna 2 is set at 115° with vertical and horizontal polarization; and Antenna 3 is set at 135° with vertical polarization (90° from antenna 1). The left-side antennas are numbered 4-6: Antenna 4 is set at 135° with vertical polarization; Antenna 5 is set at 85° with dual polarization; and Antenna 6 is set at 45° with

10

vertical polarization (90° from antenna 4).

Since the fan-beams illuminate large, elongated areas on the surface simultaneously, methods had to be devised to resolve the received power from each antenna beam as a function of spatial resolution. In addition, the antennas were illuminated in such a way to ensure collocated σ_0 measurements from each beam with 25 km spatial resolution on an earth-located grid (Table 2.1).

Quantity	Requirement	Applicable Range
Wind Speed	2 m s^{-1} (RMS) and 10%	3-20 m s^{-1} and 20-30 m s^{-1}
Wind Direction	20° (RMS) closest ambiguity	3-30 m s^{-1}
Spatial Resolution	25 km and 50 km	NRCS cells and Wind vector cells
Location Accuracy	25 km (RMS) and 10 km (RMS)	Absolute and Relative
Coverage	90% Ice-free ocean Every two days	

Table 2.1. Major NSCAT technical mission requirements [Naderi et al. 1991].

Different techniques were used to achieve along-beam and along-track resolution. The technique to achieve the desired along-beam resolution used a Doppler filtering technique utilizing the fact that the radar echo reflected from the ocean surface was Doppler shifted due to the motion of the spacecraft relative to the earth surface. The return echos from different portions of the antenna footprint had different Doppler shifts, with a larger shift at far swath

11

(Fig. 2.5). The differences in Doppler shift were used to filter the returned echos into along-beam resolution "cells." The 600 km wide swath on each side of the sub-satellite track was resolved into 24 "σ_0 cells" each having 25 km spatial resolution.

Along-track resolution used measurement timing such that the centers of cells measured by each antenna beam were approximately collocated with a spatial resolution of 25 km. The NSCAT host spacecraft, ADEOS, flew in a 795 km, 101 min polar orbit, which resulted in a sub-satellite velocity of approximately 6.7 km s^{-1}. The 25 km resolution was achieved by making measurements at each azimuth once every 3.74 s, which is the time for the sub-satellite point to move 25 km. During each 3.74 s measurement cycle, 0.468 s were allocated for each antenna beam to make σ_0 measurements.

Wind retrieval involved inversion of the geophysical model function and identification and ranking of the "near" solutions obtained by solving the over-determined system for wind speed and direction. The NSCAT wind retrieval technique used a maximum likelihood estimation of wind velocity based on the measured σ_0 and estimated noise data. Typically 16 σ_0 estimates were available for each 50 X 50 km wind vector cell on the ocean surface (each cell was 25 X 25 km and cells were available from each of the four antenna beams). Solution of the geophysical function model involved determining the wind speeds and directions that were statistically consistent with the 16 measured, but noisy, σ_0 values. The process yielded a set of possible wind vector solutions, known as wind vector ambiguities, that had similar wind speeds at different directions.

The NSCAT ambiguity removal algorithm used a modified median filter technique to select a unique wind vector from the set of ambiguous vectors. The wind retrieval algorithm

computed a set of wind vectors together with their relative likelihoods for each wind vector cell. The solution believed to be closest to the true wind was called the "closest" solution and all the wind vector solutions found in each wind vector cell (WVC) were referred to as "ambiguities." Two to six ambiguities were found per WVC. Approximately 60% of the most likely ambiguities were the closest solution and around 30% of the most likely ambiguities were in the opposite direction to the closest solution. The objective of the ambiguity removal algorithm was to choose the "closest" solution from the list of "ambiguities." This objective was equivalent to detecting cases where the ambiguity with the highest likelihood was not the closest solution, and selecting the closest solution from the rest of the ambiguities. The ambiguity removal algorithm began with the field of "most likely" wind vectors (representing the best fit to the geophysical model function) as derived from the wind retrieval algorithm. The wind vectors in a 7 X 7 filter window determined a median vector for the center cell. The median vector was compared to the ambiguities in that cell. The closest ambiguity to the median vector was selected for use in the next iteration.

C. PROCEDURES FOR CONVERTING NSCAT DATA TO TC-RELATIVE WINDS

Level 2.0 data were used for this research and were retrieved via File Transfer Protocol (FTP) from the Jet Propulsion Laboratory. All of the data were from the reprocessed data set, April 1997, where wind values are those determined at 10 m above the ocean surface. Only those western North Pacific tropical cyclones attaining tropical cyclone intensity of greater than 40 kt between 15 September 1996 and 30 June 1997 (NSCAT lifetime) were studied for wind profile determination. The following 1996 TCs were used:

13

25, 26, 28, 29, 36 (for fixes only), and 42. TC 32 was omitted due to the large land effects on the wind data caused by the Philippines. TC 36 was used for evaluating fix locations only because the radial profile data displayed a flat curve that violated conditions for a mathematical solution. The 1997 TCs used were 02, 06, 07, and 08. The best-track data from JTWC were used to determine the position of the TC with respect to the NSCAT swath coverage. The best-track file provides the TC positions every six hours with the direction and speed of the storm, and the estimated intensity.

Mark Boothe created a program that would search the best-track data base and the NSCAT revolutions and locate TC centers within 15° lat. of swath data. The program then creates a data file of only the NSCAT wind values within 15° lat. In this same program, the NSCAT wind vectors are converted to east-west (u) and north-south (v) components. The u and v components are then converted to storm relative (subscript r) radial (u_r) and tangential (v_r) components, with the storm translation interpolated to the time of the satellite overpass. The u_r and v_r components are calculated along 24 radials around the storm so that each represents a 15° sector (Fig. 2.6). Selecting particular sectors distinguishes between right and left sides or forward and rear sectors of the TC.
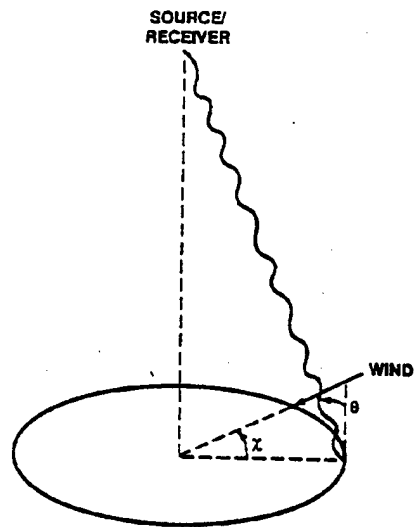
Figure 2.1. Sketch of the scattering geometry. Incidence angle θ is measured in the plane normal to the mean ocean surface. Azimuth angle χ is the angle (in the plane of the mean surface) between the wind vector and the projection of the radar illumination vector [Naderi et al. 1991].
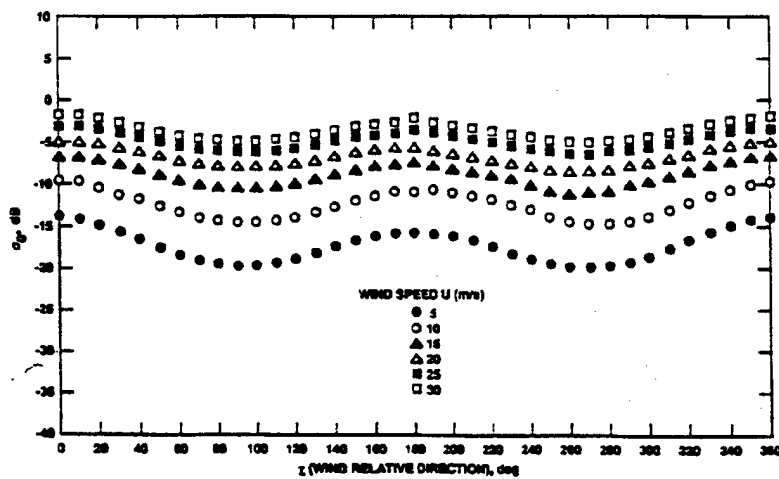

Figure 2.2. Normalized radar cross section as a function of azimuth angle (h-pol, $\theta = 30°$) for several wind speeds [Naderi et al. 1991].
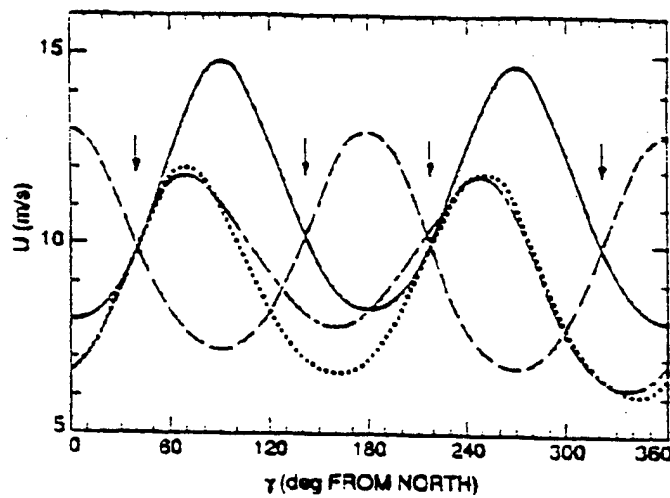
15

Figure 2.3. Loci of possible vector winds associated with collocated noise-free σ_0 measurements obtained from antennas at various azimuth angles. Heavy solid line: antenna angle of 0° (v-pol); dashed line: angle of 90° (v-pol); light solid line: angle of 25° (v-pol); dotted line: angle of 25° (h-pol). Arrows indicate solutions obtained using only the antennas at 0° and 90° [Naderi et al. 1991].
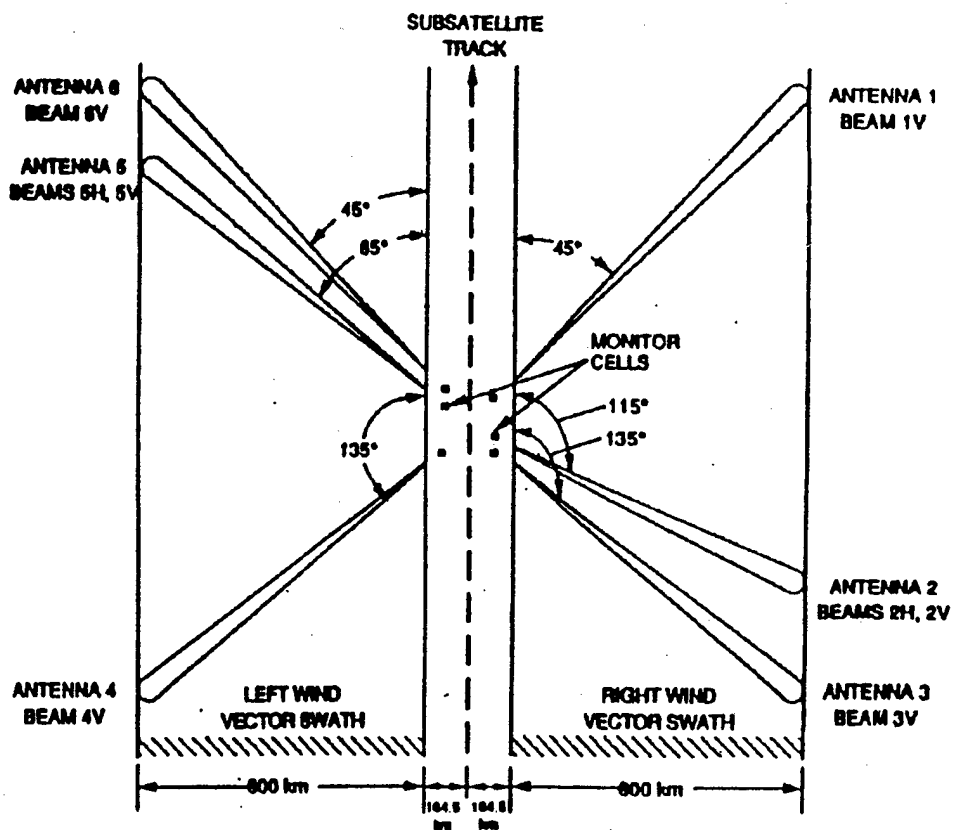
16

NSCAT ANTENNA ILLUMINATION PATTERN

Figure 2.4. NSCAT antenna illumination pattern [Naderi et al. 1991].
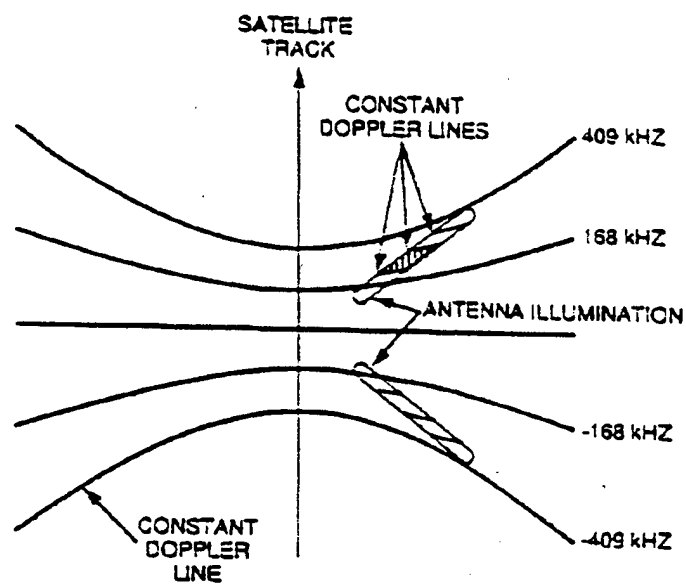
Figure 2.5. Overlay of the scatterometer fan beams on constant Doppler lines. The intersection of these lines with the beams' footprints define Doppler cells within which wind vectors are measured [Naderi et al. 1991].

RIGHT

FRONT

REAR

LEFT

STORM MOTION

Figure 2.6. Schematic of quadrants analyzed. The front, right, rear, and left sectors consist of five sectors each for 75° sectors. The gaps between the quadrants are sectors 4, 10, 16, and 22, which were ignored to avoid overlapping the data.

19

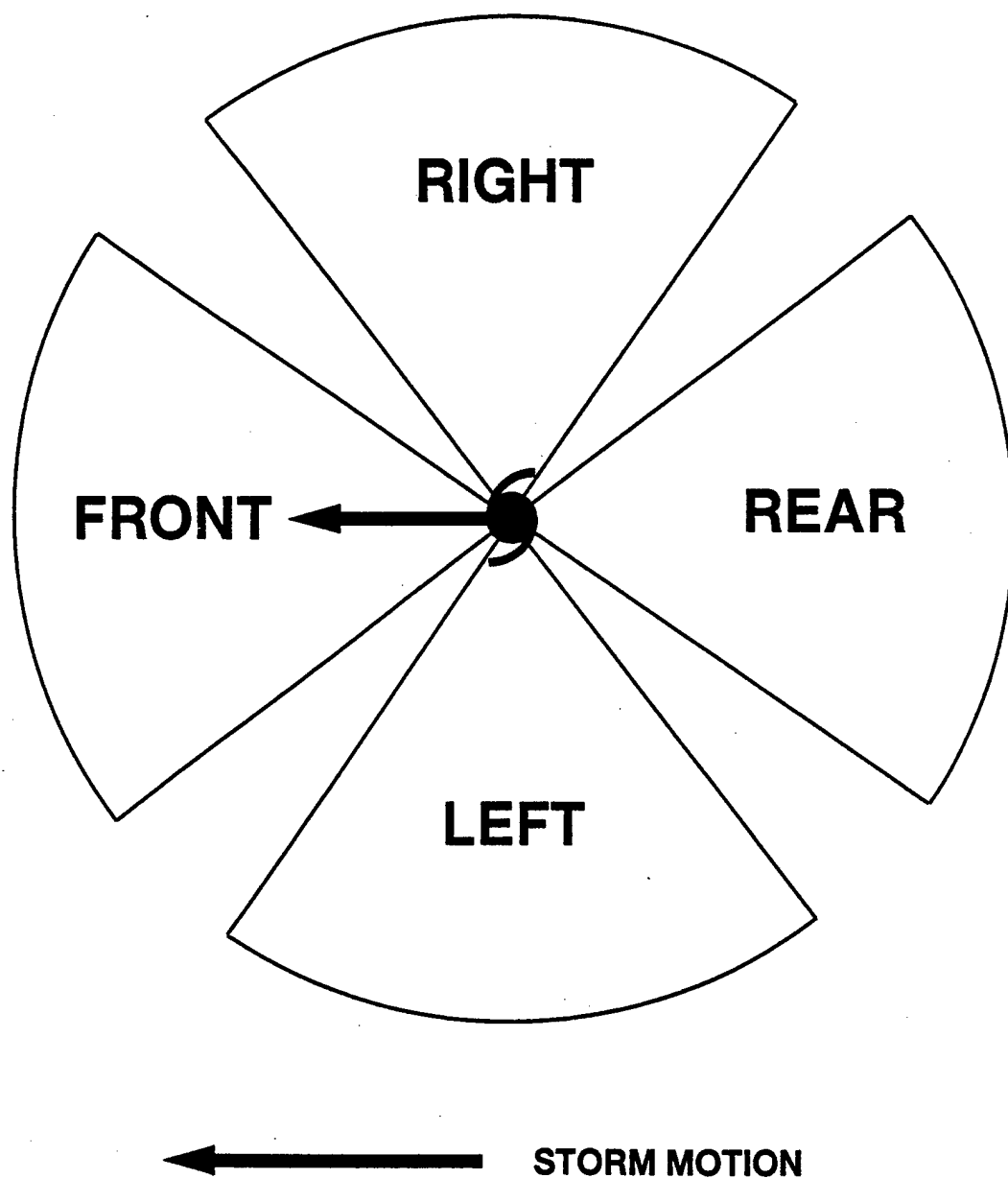# III. CHARACTERIZATION OF NSCAT DATA COVERAGE AND QUALITY

A. DESIRED PARAMETERS/COVERAGE/QUALITY

The most desirable NSCAT swaths are those in which the TC center is fully enclosed by wind measurements and the apparently correct wind vector solutions are selected. With this type of coverage, a better radial profile can be acquired and the accuracy of the best-track position can be objectively checked.

The tangential wind profiles should have continuous data and little spread in the radial plots that create a smooth curve of higher wind speeds inward that decrease outward. Due to the 400 km swath gap, sometimes not all 24 radial sectors will have data. The same will happen if the TC is located to the right or left of both NSCAT swaths. It is possible for only one quadrant to contain wind data if the storm direction is parallel or perpendicular to the satellite direction.

In the TC region with rapidly changing wind directions, an incorrect wind direction solution in the NSCAT will be fairly obvious. Large discrepancies may be found near the storm centers, land, and the edges of the swaths. Near the storm center, heavy rain scatters the signal and decreases the returned signal. Fresh rainwater on the ocean surface will cause a smoothing of the surface by tending to dampen the ripples. Noisy radial profiles will result from incorrect solutions, which will make analysis of the TC wind structure less reliable, more subjective, or even impossible.

When possible, an outer limit of cyclonic wind (R_0) estimate was subjectively determined where the winds changed from cyclonic to anticyclonic curvature. The rule was

21

to use wind vectors where diffluence was indicated near the cyclonic/anticyclonic boundary.

B.   EVALUATION OF NSCAT DATA COVERAGE AND QUALITY

The TC center position was evaluated by examining each swath and categorizing the confidence in the fix position relative to the wind center in the NSCAT data (Table 3.1). The

TC	High	Medium	Low
Tom 2596	4	3	4
Violet 2696	2	4	5
Yates 2896	0	4	5
Zane 2996	2	0	5
Dale 3696	0	3	4
Fern 4296	3	6	6
Isa 0297	2	7	7
Marie 0697	0	0	2
Nestor 0797	0	3	8
Opal 0897	1	0	3
Totals	14	30	49

Table 3.1. Number of cases with high, medium, or low levels of position confidence (see text for description) for TCs observed by NSCAT. The number following the TC name in the first column is assigned by JTWC.

following position-confidence criteria were used: high--TC center position fully enclosed by wind data without being on the edge of the swath (Fig. 3.1), i.e., that a TC position could be made with high confidence, and wind vector solutions were representative of the flow into a TC; medium--TC center enclosed by swath, although with apparent erroneous wind solutions or perhaps some land effects, or an apparent center between the two swaths with

22

appropriate wind solutions to interpolate the TC center position (Fig. 3.2); and low--TC center to the left or right of both swaths, significant number of incorrect wind solutions are apparent, or large land effects.

Comparing the JTWC best-track position with the NSCAT wind center, a total of ten center relocations could have potentially been made. Because the NSCAT revolution times did not coincide with the JTWC warning times, the TC positions were interpolated between the JTWC 6-h positions. Of the ten TCs that might have been relocated, eight could be accomplished with a high amount of confidence (centers enclosed by wind data). TY Tom (2596) had the highest number of potential relocations with four (NSCAT revolution number, degrees latitude relocated, JTWC intensity estimate in kt): 484, 1.0°, 45; 491, 1.4°, 45; 505, 2.0°, 45; 519, 1.7°, 45. Notice that this series of potential relocations occurred over a period of about 2.5 days when the storm intensity was consistently at 45 kt. TC 2996 had one potential relocation: 578, 0.6° lat. when the TC was strong (100 kt). TC Fern (4296) had three potential relocations: 1811, 1.0°, 40; 1819, 1.0°, 45; and 1890, 2.0°, 75. In the first two cases, TC Fern was only at 40-45 kt, so that more relocations might be expected if the storm is not as well organized. Although several other positions could have been relocated, their location relative to the NSCAT data (i.e., between swaths) meant little confidence could be placed in these relocations. Because the tendency for TCs to "wobble" along their track could not accurately be accounted for, these results should be viewed as potentially containing small errors.

The NSCAT data coverage was also investigated by comparing the number of 6-h warning periods when the TC intensity was greater than 40 kt and the (potential --recall that

JTWC did not have access to NSCAT) number of these warnings that might have provided a fix position with a confidence level of high or medium (Table 3.2). The average percent fix coverage was 13 (Table 3.2) and TC Fern had the highest percent coverage at 28. Notice that Marie had no NSCAT fixes during the 20 warnings (five days).

TC	Warnings	Fixes	Percent
Tom 2596	40	7	18
Violet 2696	44	6	14
Yates 2896	43	4	9
Zane 2996	39	2	5
Dale 3696	34	3	9
Fern 4296	32	9	28
Isa 0297	46	9	20
Marie 0697	20	0	0
Nestor 0797	31	3	10
Opal 0897	21	1	5
Totals	350	44	13

Table 3.2. Number of warnings for TCs (see text for description) with intensity ≥40 kt and the potential number of NSCAT fixes during the warning period. The number following the TC name in the first column is assigned by JTWC.

The number of swaths with wind profiles that would allow the TC wind structure to be evaluated was also compared with the number of warnings (Table 3.3). A swath with good wind profile coverage is defined as one with NSCAT wind data between 300 and 500 n mi (see Chapter IV) in at least one quadrant.

24

TC	Warnings	Structure	Percent
Tom 2596	40	11	28
Violet 2696	44	11	25
Yates 2896	43	9	21
Zane 2996	39	7	18
Dale 3696	34	7	21
Fern 4296	32	15	47
Isa 0297	46	16	35
Marie 0697	20	2	10
Nestor 0797	31	11	35
Opal 0897	21	4	19
Totals	350	93	27

Table 3.3. Number of warnings when the TC intensity ≥40 kt compared with the number of NSCAT swaths with at least one quadrant wind profile during the 6-h warning period. The number following the TC name in the first column is assigned by JTWC.

The average wind profile coverage was 27%, which is 14% higher than the average coverage for fixes because the TC center does not have to be in the center or between swaths in order to acquire a radial profile. TC Fern also had the highest wind profile coverage with 47%. Marie had the lowest percent coverage with 10%.

A R_0 value was estimated in 71 of 93 swaths. The outer limit of cyclonic wind could (R_0) not be determined for every available swath, primarily because a location along the NSCAT swath where the winds became anticyclonic could not be found. For example, the TCs at lower latitudes in the monsoon trough are embedded in a cyclonic circulation. Farther north, the TCs may be moving into a stronger environmental flow so that the size of the gale-

force winds increases. These R_0 values inferred from the cyclonic to anticyclonic direction change locations will be compared with the values inferred from the wind profile solution in Chapter IV.
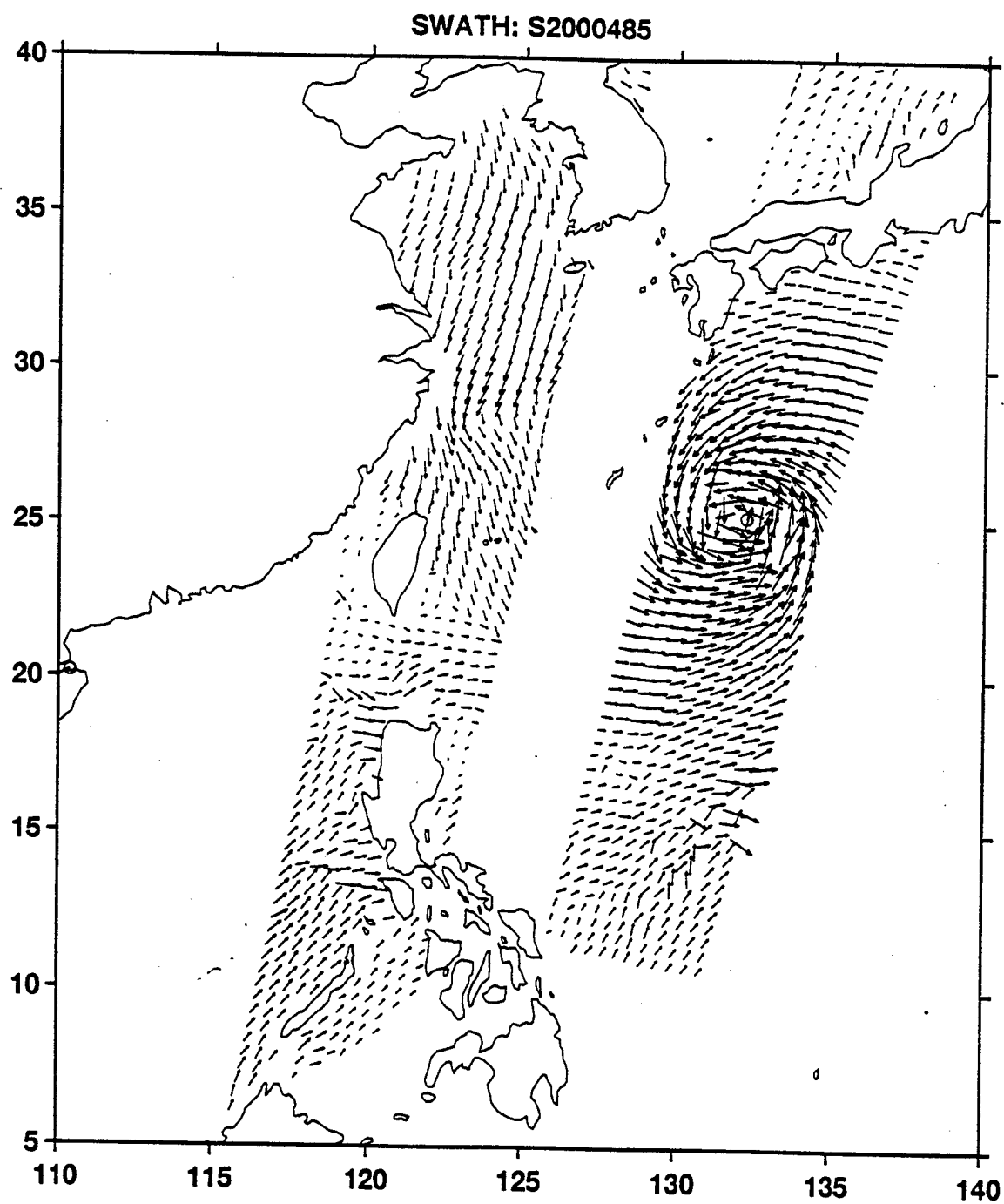
Figure 3.1. Example of NSCAT swath with a high confidence TC center position (see text for description).
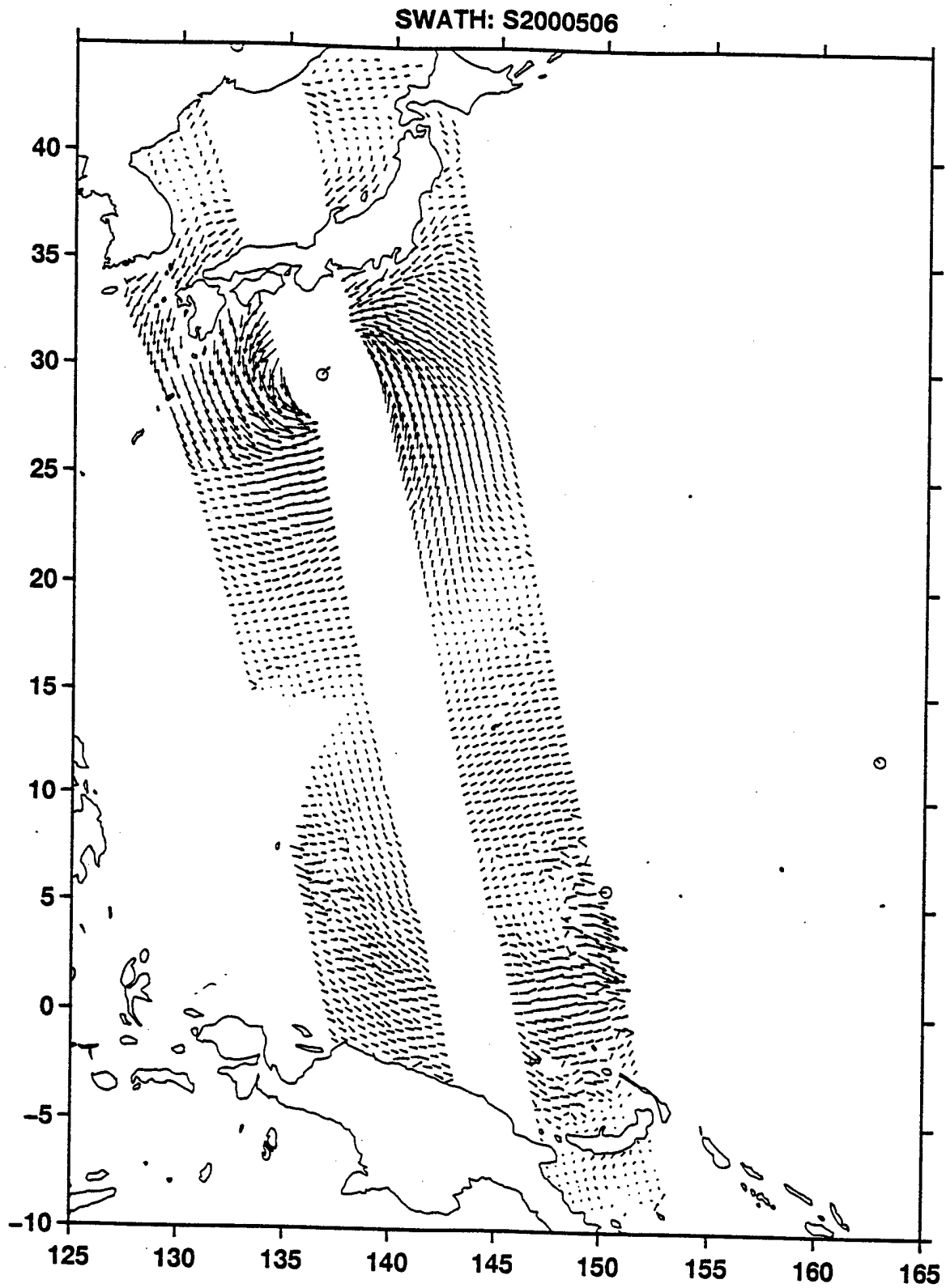
SWATH: S2000506

Figure 3.2. NSCAT swath as in Fig. 3.1, except for a medium confidence TC center position between two swaths.
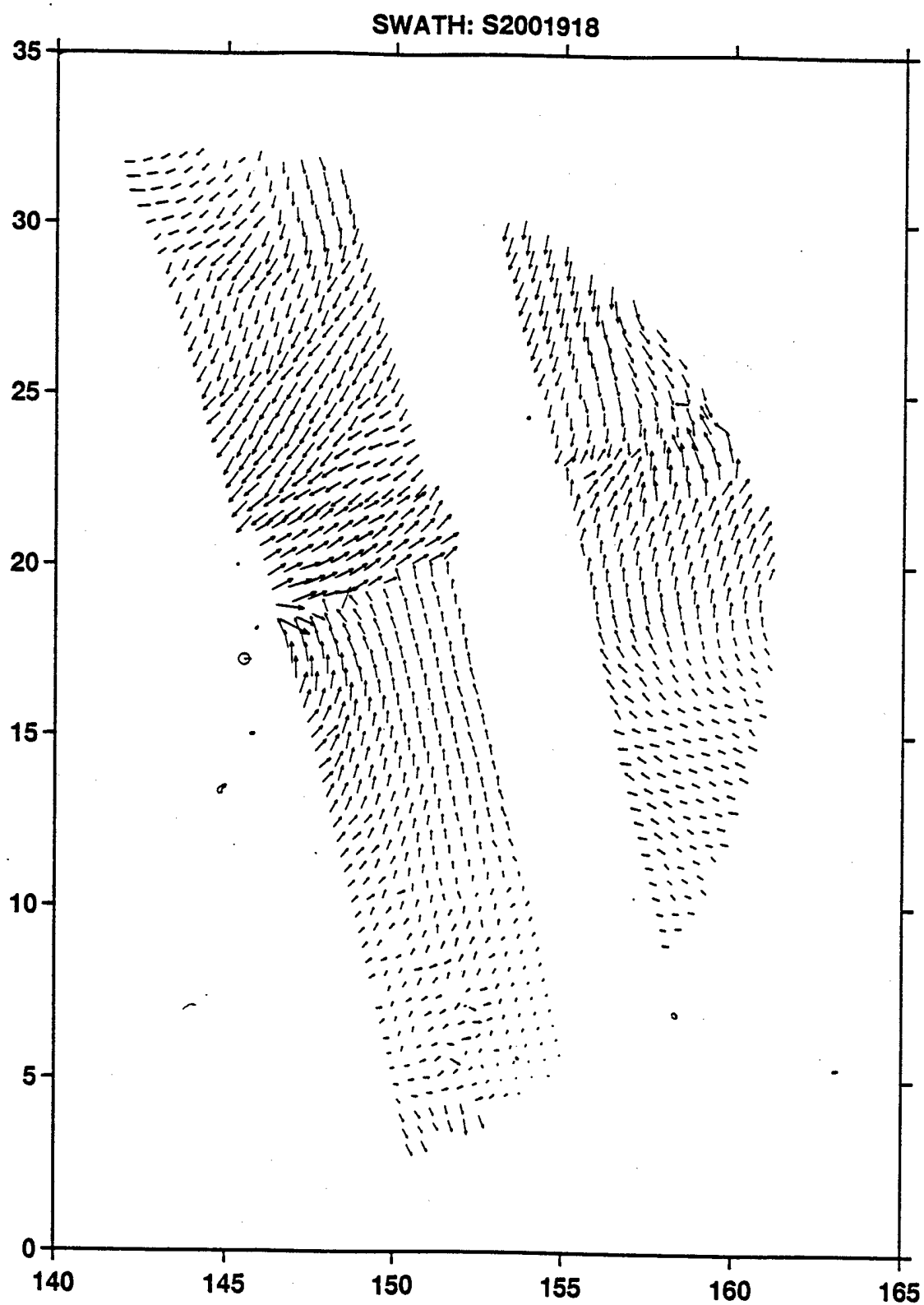
28

Figure 3.3. Example of NSCAT swath with a low confidence TC center position left of both swaths with incorrect wind vector solutions.

29

IV. WIND RADII ESTIMATION

A.   DESCRIPTION

Because the scale of even the largest TCs (~1000 km) is small in comparison with the radius of the Earth (~10,000 km), the absolute angular momentum (M_a) of a parcel at distance r from the center of a TC is reasonably approximated by

$$M_a = rv + \frac{1}{2} f_0 r^2, \tag{4.1}$$

where v is the tangential wind and f_0 is the value of the Coriolis parameter at the latitude of the TC center. Consider an idealized situation in which the TC is not moving, the wind field is perfectly axisymmetric and steady (i.e., there is dynamic equilibrium). If there is also an absence of friction throughout the inflow layer, the absolute angular momentum of parcels in the inflow layer would be conserved. Given all these conditions, the tangential wind speed at any instant in time at any radius between the outer edge of the TC (R_0), where the tangential wind speed is zero, and the radius of maximum wind (R_m) would be given by

$$v(r) = \frac{M_a}{r} - \frac{1}{2} f_0 r, \tag{4.2}$$

where M_a can be determined from (4.1) given the tangential wind speed at any radius between R_0 and R_m. If the maximum wind speed (V_m) and R_m are known, these values may be inserted in (4.2) to solve for M_a, and then the complete profile could be specified. Alternately, if the outer boundary R_0 is known, and given that $v(R_0) = 0$ by definition, then

31

$$M_a = \frac{1}{2} f_0 R_0^2.$$

(4.3)

The first and second term on the right side of (4.2) represent the contribution to TC tangential wind due to the conservation of parcel angular momentum relative to the Earth surface, and the conservation of angular momentum imparted by the rotation of the Earth, respectively.

Because significant turbulence-induced momentum from the TC inflow layer is transferred to the Earth surface, the parcel M_a is not conserved, but rather decreases with decreasing radius between R_0 and R_m. A simplistic and traditional way to account for this momentum loss is to alter the form of the first term on the right side of (4.2) so that the tangential wind is now given by

$$v(r) = \frac{M}{r^x} - \frac{1}{2} f_0 r,$$

(4.4)

where x is positive and less than one, and M is given by

$$M = \frac{1}{2} f_0 R_0^{1+x},$$

(4.5)

where the outer boundary condition of $v(R_0) = 0$ has been applied as in (4.3). Analysis of data from aircraft reconnaissance into TCs at flight levels above the boundary layer has shown that within radial distances at which the Coriolis term in (4.4) may be ignored (<200 km), a constant value of x between 0.3 and 0.5 provides a good fit to observed TC tangential wind profiles (Riehl 1963).

Carr and Elsberry (1997) proposed using (4.4) with a constant x = 0.4 to specify mid-

tropospheric tangential wind structure for the outer portion of the TC for the specific purpose of modeling TC beta-effect propagation. They did not address the inner-core structure aspects of (4.4), since beta-effect propagation has been shown to be insensitive to TC wind structure inside about 300 km (Fiorino and Elsberry 1989).

A direct application of (4.4) to specify TC "surface" (versus the lower-to-middle portion of the troposphere considered by Riehl (1963) and Carr and Elsberry (1997) over the entire region from R_m to R_0 is not justifiable for a number of reasons. First, the first term on the right side of (4.4) with x held constant provides only a very crude parameterization for the complex effects of turbulent friction in the boundary layer. Thus, it is very unlikely that a tangential wind profile given by (4.4) for any single value of x can account for the effects of friction with sufficient realism to provide representative values of tangential wind at all radii from R_m to R_0. A second concern is using the TC center latitude to determine the value of Coriolis in (4.4) throughout the TC circulation, particularly at large radii. Recall that the validity of (4.3) depends on the assumptions of axisymmetry, steady structure, and no motion. Significant asymmetries may be present in the surface wind field at larger radii. The cyclonic circulation of a TC is largest in the boundary layer and decreases with elevation. Also, the TC is usually moving at a significant speed compared to the tangential wind speed of parcels at larger radii. Finally, the wind structure of the TC is usually not steady, even with respect to a coordinate system moving with the TC. As a result of the above factors, the average effect of Coriolis torque on all parcels throughout the boundary layer in a real TC may not be well represented by the Coriolis value at the center of the TC.

Although a direct application of (4.4) may not be justifiable for the purpose of this

33

project, the underlying physical basis of the formula makes it very desirable retain the same functional properties whatever tangential wind formula is ultimately used. Not only does (4.4) provide for a definite TC extent (R_0), it produces tangential wind profiles that have a predominantly linear dependence on radius far from the TC center, which is an expected effect of Coriolis torque. At small distances from the center, a nonlinear dependence on radius is an expected effect of fictionally-adjusted relative momentum conservation. This approach seems more preferable than the use of purely empirical formulas that have no physical basis, and produce highly unrealistic results (e.g., inappropriate curvature just outside the radius of maximum wind, exponential decay with radius, and, ironically, infinite size).

Thus, the following adaptation of (4.4) will be used here: (1) For radial distances greater than 5° latitude (300 n mi), the parameter x will be set to zero to give

$$v(r) = M - \frac{1}{2}f_0 r, \qquad (4.6)$$

which has the linear dependence on radius observed in radial profiles of tangential wind obtained from scatterometer data. In lieu of any guidance to the contrary, the value of the Coriolis parameter f_0 is calculated from the latitude of the TC center. The linear profile given by (4.6) may be scaled to conform to the outer tangential wind profile of a particular TC via knowledge of the tangential wind (V_1) at some radius R_1, which in this study was chosen to be 300 n mi or 5° latitude. Substituting V_1 and R_1 into (4.6) results in

$$M = V_1 + \frac{1}{2}f_0 R_1. \qquad (4.7)$$

The profile given by (4.6) applies from radius R_1 out to the radius of zero wind R_0, which by

34

combining (4.6) and (4.7) is given by

$$R_0 = R_1 + 2\frac{V_1}{f_0}. \tag{4.8}$$

(2) For radial distances less than $5°$ latitude (300 n mi), a radius-dependent value of x is used in (4.4), which gives the formula

$$v(r) = \frac{M}{r^{x(r)}} - \frac{1}{2}f_0 r. \tag{4.9}$$

As in (4.6) above, the value of f_0 is determined by the latitude of the TC. The value of M is determined by

$$M = \frac{1}{2}f_0 R_0^{1+x(r)}, \tag{4.10}$$

where the same value of R_0 given by (4.8) is used here to ensure a smooth match between (4.6) and (4.9) at R_1. The dependence of x on the radius in (4.9) is chosen to be quadratic between R_1 and the radius of maximum winds (R_m), as given by

$$x(r) = x_m \frac{(R_1 - r)^2}{(R_1 - R_m)^2}, \tag{4.11}$$

where x_m is the maximum value of x at R_m. Notice that (4.11) gives a zero value for both x and its slope at R_1, which is also necessary to get a smooth match between (4.9) and (4.6) at R_1. The value of x_m in (4.11) is determined by requiring that (4.9) give a tangential wind

35

speed equal to the estimated maximum wind speed (V_m) of the TC when $r = R_m$. The necessary value of x_m must be determined iteratively by substituting into (4.11) increasing values of x_m (beginning at zero), and then substituting the resultant value of x into (4.10) and (4.9), until $v = V_m$ for $r = R_m$. Once x_m is determined, then (4.9) may be used to compute tangential wind speed at any radius between R_1 and R_m after first computing the value of x and M at that radius using (4.11) and (4.10), respectively.

Additional assumptions are that the V_m from Dvorak analysis is correct, and that R_m is 15 n mi. When varied slightly, these two assumptions have only small effects on the calculated R_{35} and R_{50}.

B.   WIND RADII EVALUATION

The wind structure on the front and rear sectors of Fig. 2.6 is evaluated in terms of storm-relative tangential wind radial profiles whenever NSCAT observations are available in those sectors. The radius within the linear profile region for which tangential wind speed in knots is to be extracted is fixed at 300 n mi. This radius is selected because the wind data inside 300 n mi are more likely to be inside the linear portion of the wind profile, subject to a higher likelihood of rain contamination, and the wind values between 300-500 n mi (good linear representation) could be used as a guide for selecting the 300 n mi wind speed value. Beyond 500 n mi, the values become more scattered due to the higher probability of being affected by the environmental flow. A total of 19 front quadrants and 17 rear quadrants are analyzed (Fig. 4.1).

Evaluating the wind structure on the right and left sides of the TCs is more complicated because the NSCAT observations include the environmental flow as well as the

36

symmetric TC vortex represented by (4.9). As a first approximation to the environmental flow effect, the storm-relative winds are used on the right and left sides. The same criteria for the front and rear sides was used for determining the 300 n mi wind speed value. A total of 22 right quadrants and 20 left quadrants were analyzed.

A total of 78 quadrants out of a possible 344 quadrants (or 29%) had a TC in or near the NSCAT swath. This means there were 266 quadrants deemed either "not analyzable" (Fig. 4.2) or "not available." The 72 "not analyzable" profiles are those that do not appear to have a linear segment in which the outer wind speed was less than the inner wind speed, and thus do not appear to represent a cyclonic storm in the 300-500 n mi radii. The 194 "not available" classification is assigned for those quadrants in which little or no NSCAT wind data are found to apply (4.9).

C.   COMPARISONS WITH JTWC WIND RADII

An example of the calculation of critical wind radii is given in Fig. 4.3. Notice the wind speed $V_1 = 22$ kt at $R_1 = 300$ n mi defines the outer wind profile, which decreases to zero at $R_0 = 557$ n mi. The wind profile inside 300 n mi blends smoothly with the outer profile and terminates at the specified $V_m = 115$ kt at $R_m = 15$ n mi. The critical wind radii of 35-kt and 50-kt that are indicated along the profile may be compared to the critical wind radii issued by the JTWC in their TC warning messages. As indicated in the Introduction, considerable uncertainty exists as to the reliability of the JTWC wind radii as no aircraft reconnaissance is available in the western North Pacific, and ships tend to stay out of the 35-kt wind areas. Nevertheless, this is the only information to compare with the NSCAT wind radii. The JTWC typically reports critical wind radii only in the right and left semi-circles. These two values

37

are then averaged to provide comparison values in either the front and rear sector values calculated from NSCAT observations.

All except four or five of the 19 front-quadrant comparisons (circles in Fig. 4.4) of R_{35} are well clustered around the diagonal. Similarly, the 17 rear-quadrant values (asterisks in Fig. 4.4) are distributed along the diagonal, except for two outliers. Whereas the calculated values in the front quadrant tend to be larger than the JTWC R_{35} radii, the calculated values in the rear quadrant are slightly smaller than the JTWC values.

The corresponding R_{50} comparisons (Fig. 4.5) for the front or rear quadrants clearly indicate a bias for the calculated values to be larger than the JTWC wind radii, even excluding the four extreme values in the front quadrant. Most of the calculated values are 0-20 n mi larger when the JTWC values are in the range of 30-60 n mi, and appear to be slightly larger when the JTWC values are in the range of 80-90 n mi. Since the calculated R_{35} values in Fig. 4.5 are rather well clustered about the JTWC values, and the slopes of the calculated profiles are relatively flat (x exponent equal to zero at 300 n mi), it might have been expected that the calculated values would have been too small. Perhaps the use of a constant $R_m = 15$ n mi contributed to the error. It is also possible that the estimate of the JTWC R_{50} radii in the front and the rear quadrants by averaging the right and left semi-circle values is less appropriate near the center. It is again emphasized that JTWC does not have aircraft reconnaissance to provide observations of the inner wind structure. If the JTWC forecasters use a modified Rankine profile with the V_m, R_m values and an exponent of x = 0.5, the JTWC R_{50} would tend to occur at small radii.

Since the calculated R $_{35}$ values for the right-left quadrants that are based on storm-

38

relative winds have large biases, these values are re-calculated without representing the environmental effect as the storm motion. That is, the NSCAT wind profiles in the right and left quadrants are used to calculate critical wind radii as in the front-rear quadrants and directly compared to the right and left semi-circle wind radii values from the JTWC warnings. Except for five values, the 21 right-quadrant R_{35} comparisons (circles in Fig. 4.6) are well clustered along the diagonal. Also, three calculated right-quadrant values are more than 50 n mi smaller than the largest JTWC R_{35} radii of 265 n mi. Similarly, the 20 calculated left-quadrant values (asterisks in Fig. 4.5) are distributed along the diagonal, except for four calculated values that are more than 50 n mi larger than the JTWC R_{35} values. One obvious outlier is a calculated value of 240 n mi, whereas JTWC believed the left-side R_{35} was only 90 n mi.

The R_{50} critical wind radii values are also calculated in the right and left quadrants using the same procedures for R_{35}. The right and left quadrants values in Fig. 4.7 (18 total each) again have a similar cluster around the diagonal with a clear tendency for the calculated R_{50} values to be higher than the JTWC R_{50} values as in the calculations for the front and rear quadrants (Fig. 4.5).

In summary, the calculated R_{35} values from the NSCAT wind observations in the front and rear quadrants agree within expected variations about the JTWC wind radii. However, the adjustment of the right and left NSCAT wind profiles by the storm motion to account for the environment flow results in calculated R_{35} values that are clearly biased. If this storm-motion adjustment is not made, the right and left quadrant R_{35} calculations are clustered rather well about the JTWC values. No explanation has been developed for this unusual

39

result. In both the right-left and front-rear quadrants, the calculated R_{50} values are larger than the JTWC R_{50} values.

D.   STORM SIZE COMPARISONS

Forecaster "lore" is that TCs spread out as they move into midlatitudes, which may be because the TC is moving into a stronger environmental flow so that the size of the gale-force winds increases. Based on the Carr and Elsberry (1994, 1997) wind profile and JTWC R_{35} values, Fisher (1996) found that only 29% of the TCs had an increase in R_0 during the decay phase. He found the other R_0 trends were that about 6% demonstrated a constant R_0 and the majority (about 65%) had a decrease in R_0 during the decay phase. Consequently, Fisher concluded that the tendency for the radial extent of the tangential winds associated with a TC to always increase as the TC moves into the midlatitudes may be doubtful.

The subjective analysis of the change in cyclonic to anticyclonic curvature in the NSCAT swaths revealed that in only two (Tom and Zane) of the seven analyzable TCs did the R_0 values increase as the storms moved northward. The other five (Violet, Yates, Fern, Isa, and Nestor) had nearly constant R_0 values. Marie and Opal could not be analyzed due to the low number of swaths

The calculated values of R_0 based on the NSCAT radial profiles are separated by quadrants and plotted versus the subjective R_0 values (Figs. 4.8 and 4.9). A total of 18 front, 14 rear, 17 right, and 19 left quadrant R_0 values are compared. All except five (close to equal) of the front-quadrant values (circles in Fig. 4.8) indicate the calculated R_0 values are greater than the estimated R_0 values from a change of cyclonic to anticyclonic curvature. Since the front-quadrant R_{35} values (Fig. 4.4) have a tendency to be larger than the JTWC radii, these

large R_0 values may indicate that the slope of the wind profile outward from $R_t = 300$ n mi is not steep enough. Except for 3-4 calculated rear-quadrant values, the calculated R_0 values are slightly larger than the subjectively estimated R_0 values from the curvature change. The calculated right-quadrant R_0 values (circles in Fig. 4.9) are predominantly (13 of 17) larger than the subjectively estimated R_0 values. Likewise, the calculated left-quadrant R_0 values (asterisks in Fig. 4.9) are predominantly (15 of 19) larger than the estimated R_0 values.

Unfortunately it is not clear which of the R_0 estimates is a better indicator of cyclonic extent of the TC. Carr and Elsberry (1994, 1997) do suggest the change in cyclonic to anticyclonic curvature in the 850-mb winds or cumulus cloud-drift winds is potentially a reasonable measure of TC size, when it is available. It seems clear from Figs. 4.8 and 4.9 that the calculated R_0 values from the NSCAT wind profiles as in Fig. 4.3 tend to yield larger values of cyclonic wind extent.
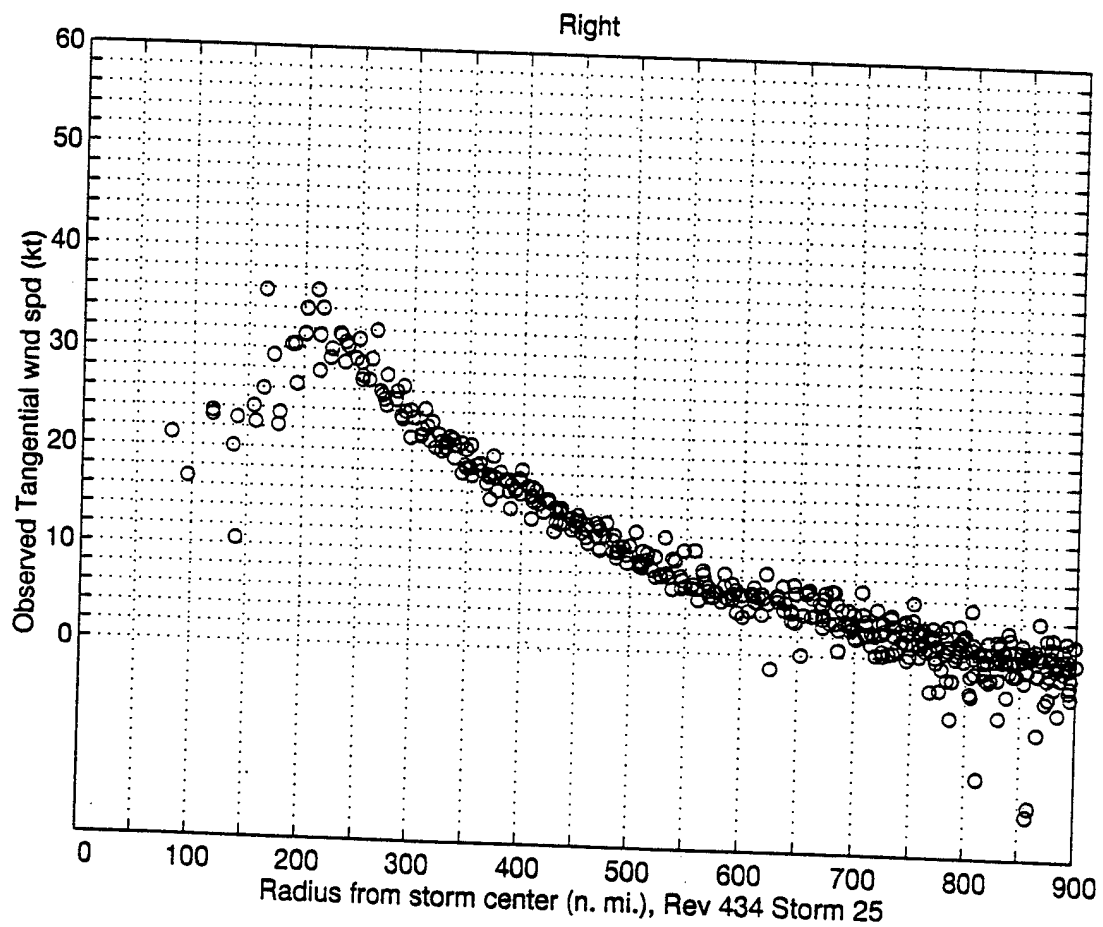
Fig. 4.1. Example of NSCAT observations prior to storm-relative calculation on right side of TY Tom that is classified as an "analyzable" tangential wind radial profile.
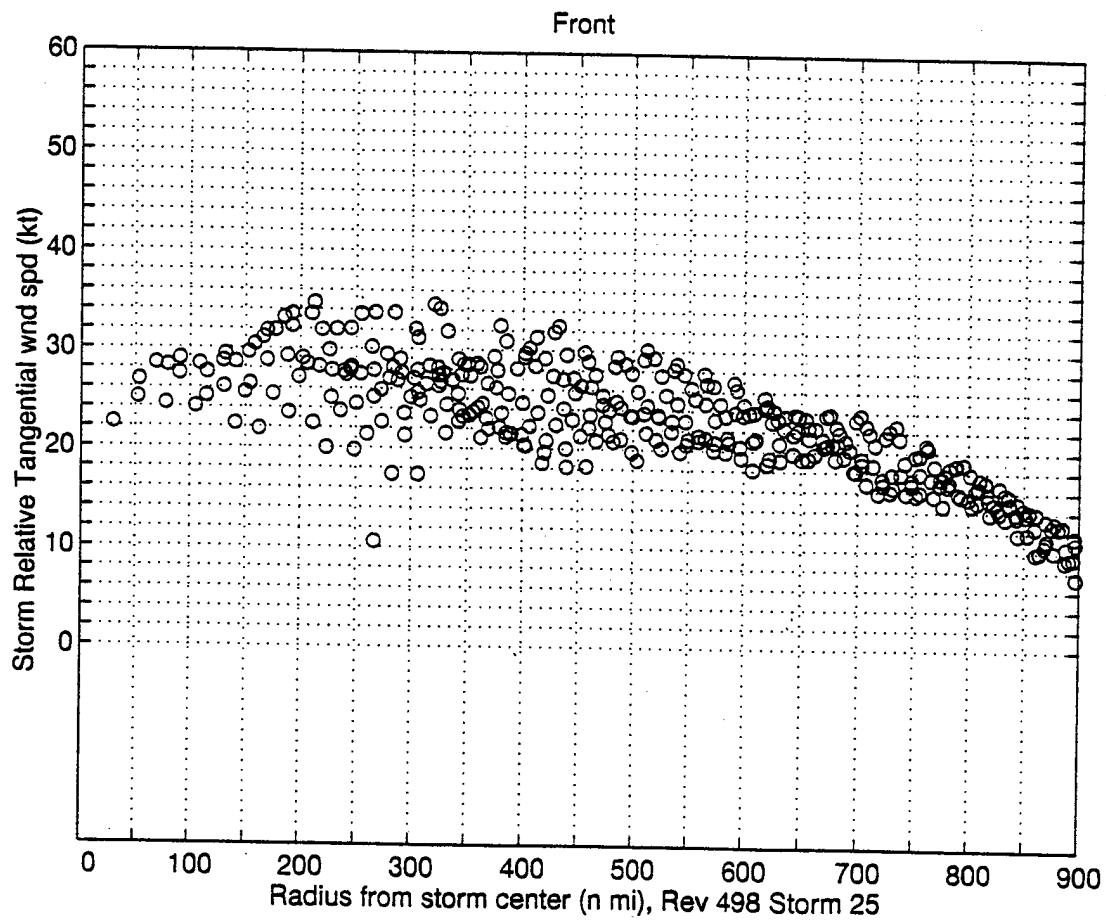
Fig. 4.2. Example of NSCAT observations in front sector of TY Tom that is classified as being a "not analyzable" radial profile (see text for description).
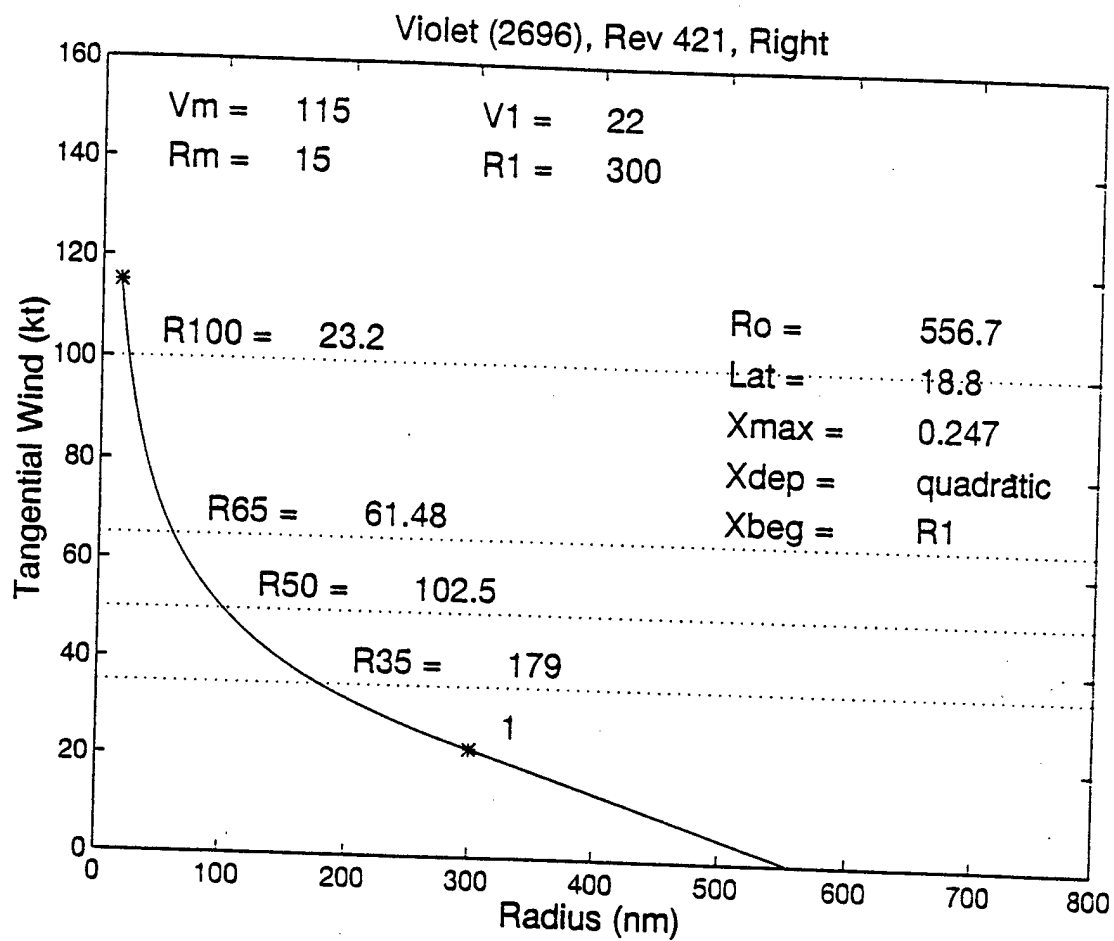
Fig. 4.3. Example of the wind profile solution and the calculated critical wind radii and R_o value for the front quadrant of TY Violet based on NSCAT wind observations in revolution 421.
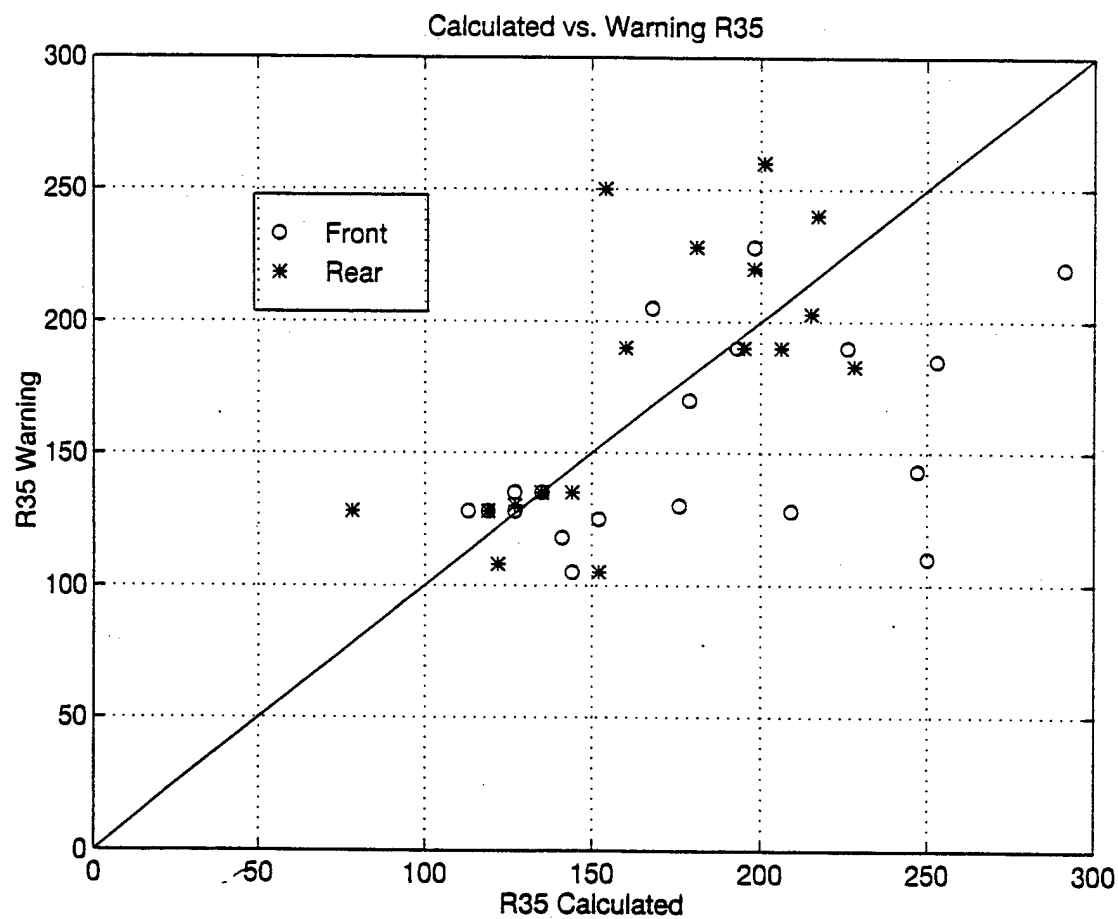
Fig. 4.4. Calculated R_{35} values from NSCAT observations in the front (circles) and rear (asterisks) quadrants compared to the JTWC R_{35} values, which are the average of the right and left semi-circle values.
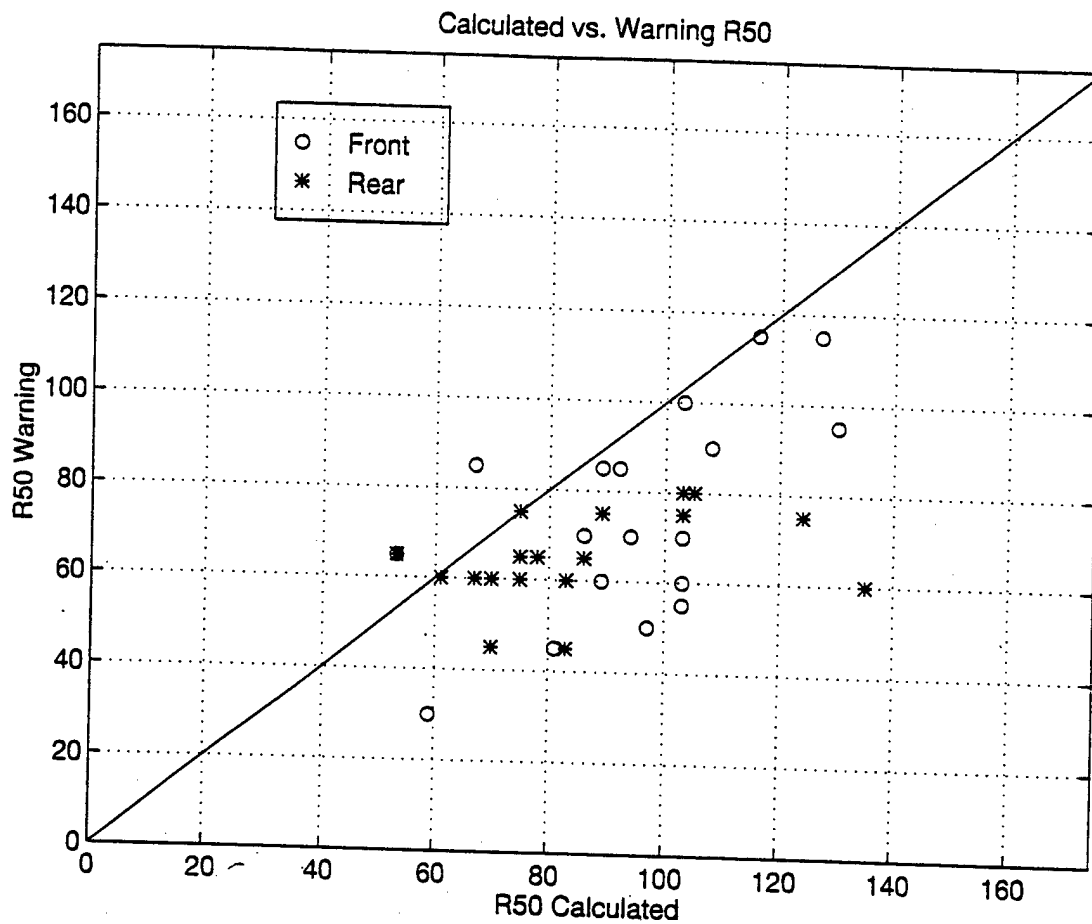
Fig. 4.5. Calculated front and rear quadrant values compared to the JTWC values as in Fig. 4.4, except for R_{50} values.
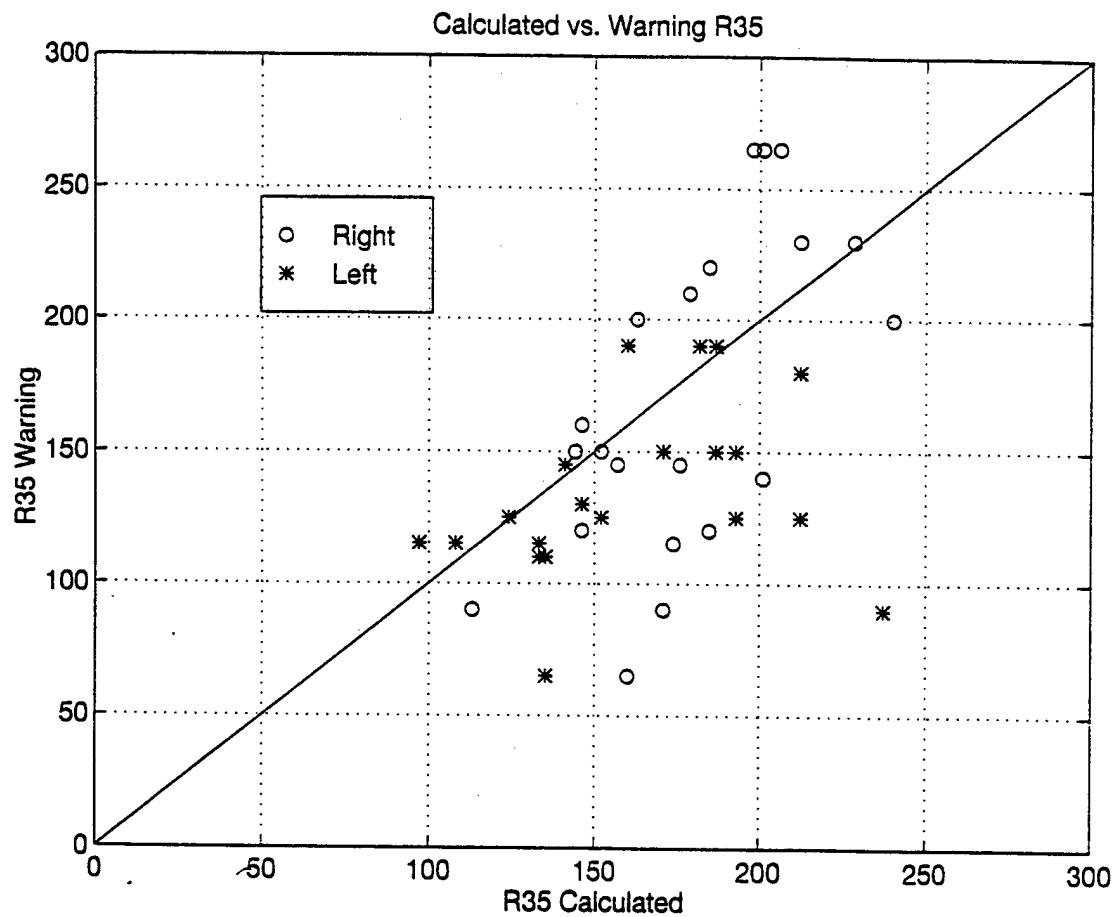
46

Fig. 4.6. Calculated R_{35} values compared to the JTWC R_{35} values as in Fig. 4.4, except for right and left quadrants without an adjustment of the NSCAT winds for storm motion.
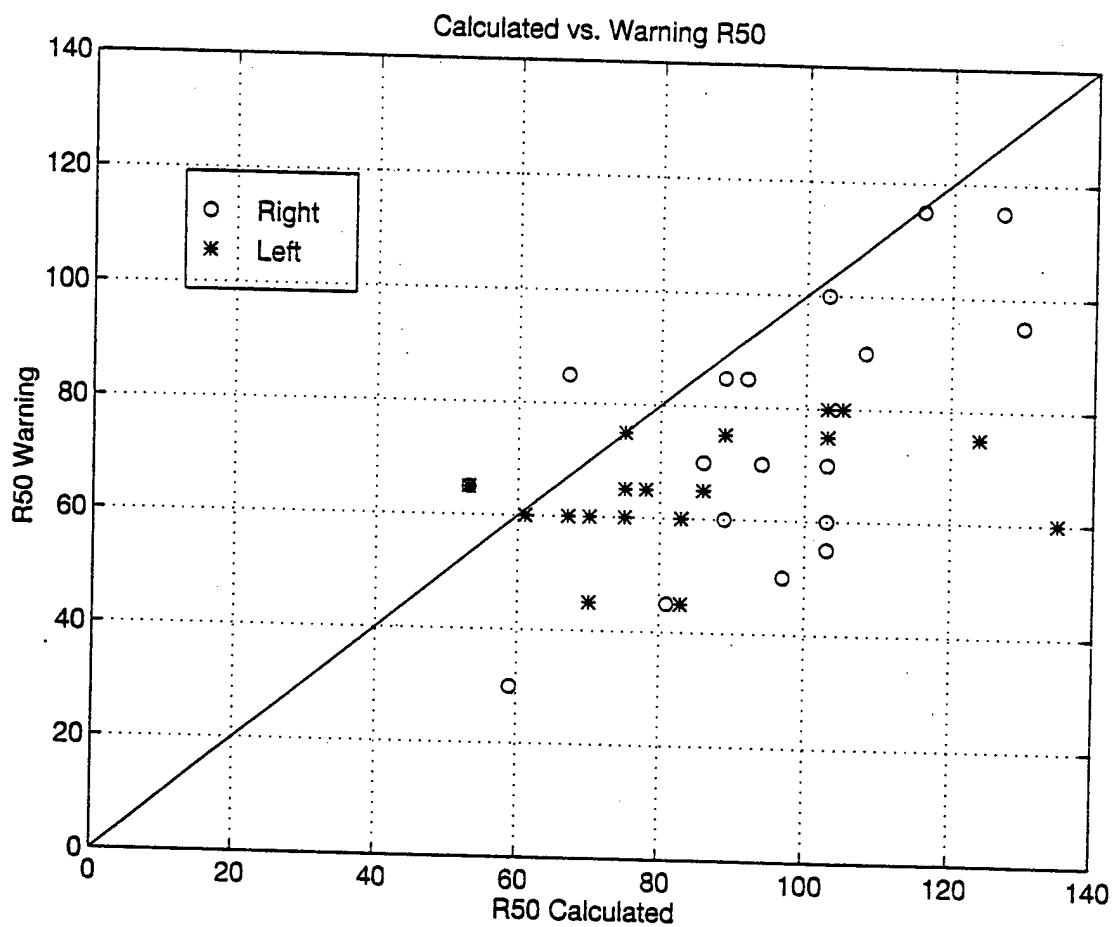
Fig. 4.7. Calculated R_{50} values compared to the JTWC R_{50} values as in Fig. 4.5, except for right and left quadrants.
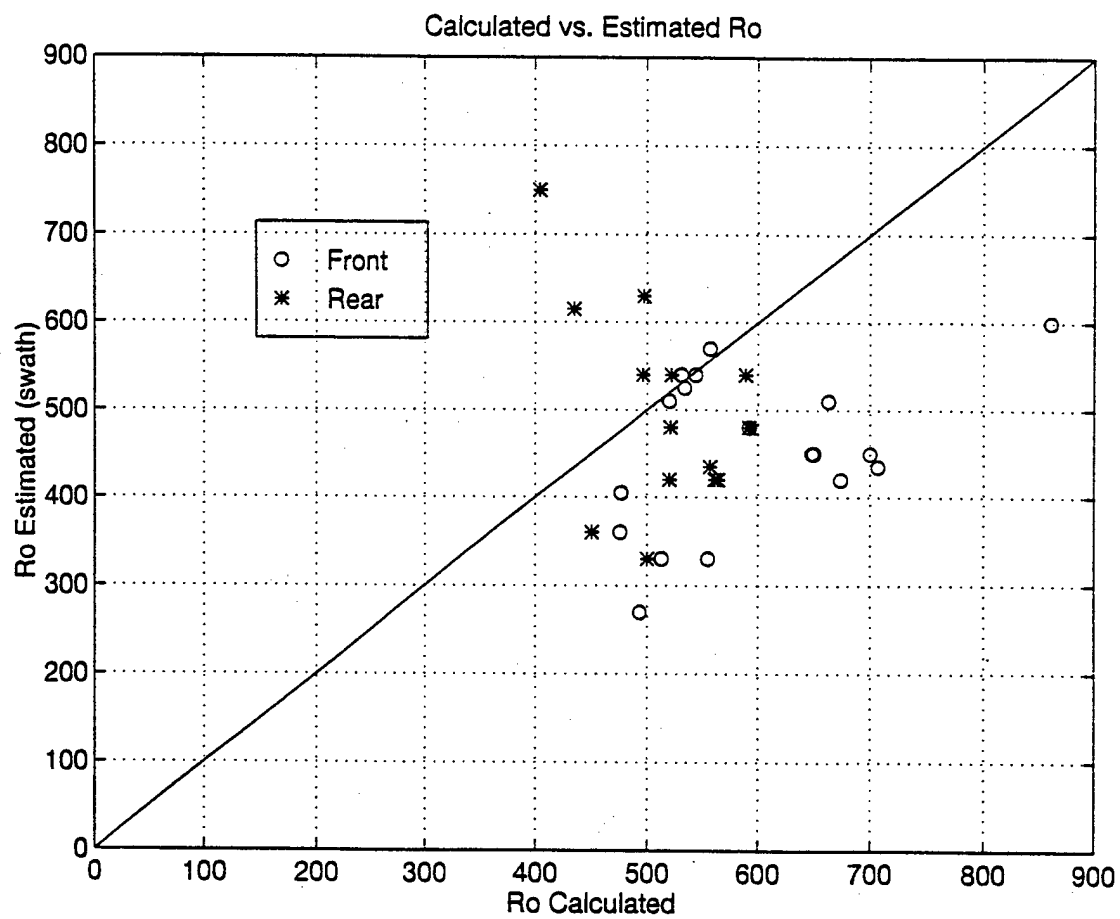
Fig. 4.8. Calculated R_0 values compared with subjective R_0 values from the change in cyclonic to anticyclonic curvature in the NSCAT wind observations in the front (circles) and rear (asterisks) quadrants.
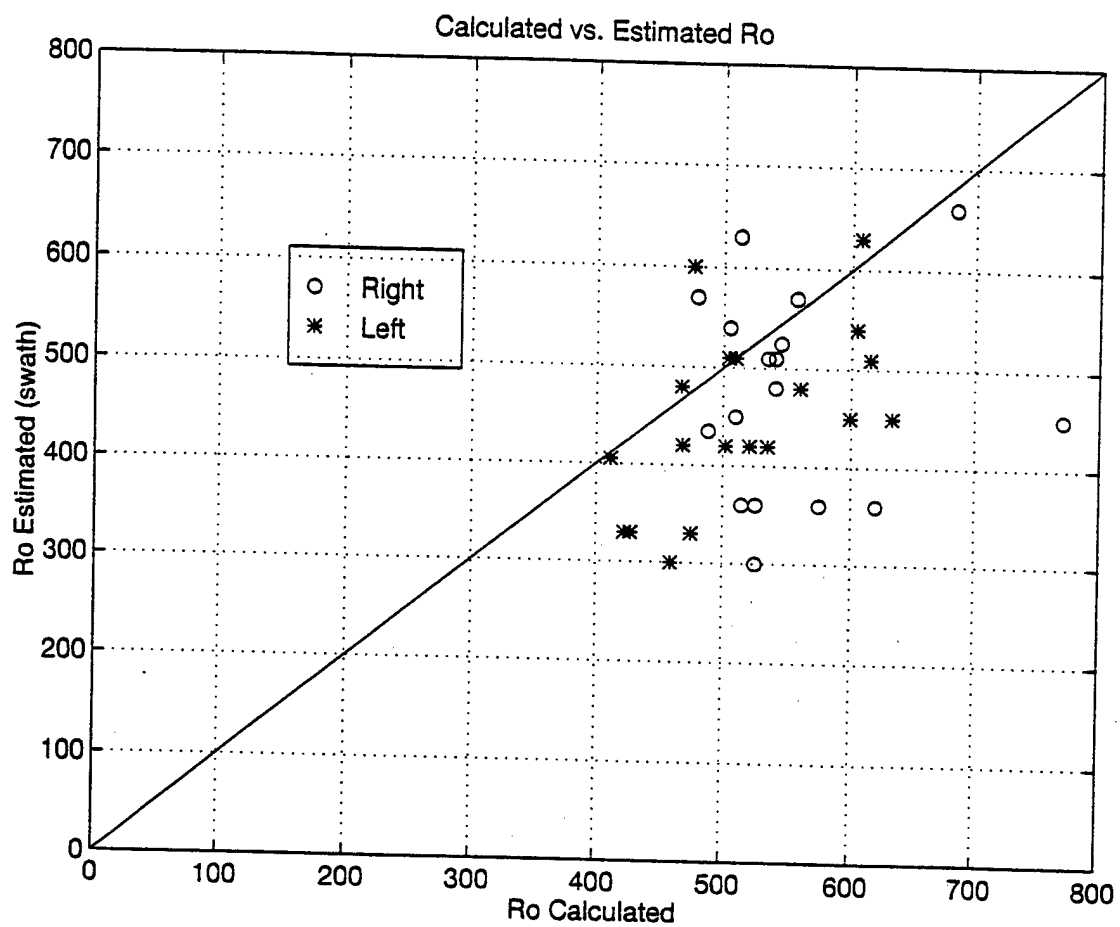
Fig. 4.9. Calculated R_0 values compared with subjective NSCAT wind curvature change estimates as in Fig. 4.8, except for the right (circles) and left (asterisks) quadrants.

V. CONCLUSIONS AND RECOMMENDATIONS

A. CONCLUSIONS

Had the NSCAT observations been available to JTWC in real-time, the NSCAT wind data would have proved useful for locating some of the TC centers, particularly in the early stages of TC development when the cirrus overcast evidently prevented the analyst from viewing low-level cloud features. In eight cases in which the NSCAT would have provided high-confidence fixes, the TC center relocations would have ranged from 0.6° lat. to 2° lat. Although the frequency with which fixes can be performed using NSCAT data is low (13% of the swaths within 15° lat. of the actual TC center would have provided fixes), such fixes are potentially valuable when the eye is not visible in the infrared imagery.

A technique is proposed for calculating critical wind radii from the NSCAT wind observations at 300 n mi. The calculated values and JTWC wind radii values have a reasonable agreement in the front and rear quadrants. The right (left) side of the TC should indicate higher (smaller) wind values due to the environmental steering flow. Since the proposed wind profile applies only to the symmetric vortex, the NSCAT wind profiles on the right and left are first adjusted to storm-relative values. When the storm motion is removed (right and left should be equal), the left-quadrant winds become too large and the right-quadrant winds become too small. Why the right and left quadrant NSCAT storm-relative tangential radial profiles did not indicate winds of equal strength is not understood. Given these biases when storm-relative NSCAT winds are used in the right and left quadrants, the profiles are recalculated without making the values storm-relative. In that case, the calculated

51

R_{35} values have a better agreement with the JTWC R_{35} radii than when storm-relative winds are used, which is the opposite of what is expected. More NSCAT observations of TC structure and of the environment are needed to separate the TC vortex from the environmental flow. Since no ground truth exists to validate these calculations, this technique should be used with caution. The ERS scatterometer data currently available to JTWC is infrequent so new data may suddenly cause the TDO to shrink or grow the outer wind radii.

The proposed profile technique for calculating where cyclonic winds go to zero (R_0) appears to have some value, although the calculated values are generally larger than the subjectively estimated R_0 values from where the NSCAT winds change from cyclonic to anticyclonic curvature. Independent calculated and estimated R_0 values would aid JTWC in estimating the approximate size of the cyclone winds, and if a large TC is indicated, then significant deviations of the TC motion from the steering current may be expected.

B.   RECOMMENDATIONS

Only western North Pacific TCs have been examined in this thesis. Perhaps NSCAT observations are available in other basins, particularly during the Southern Hemisphere season, which generally extends from December to May. It would be particularly useful to have aircraft reconnaissance observations for in situ validations of the NSCAT winds in a TC. However, such aircraft observations are generally only available in the Atlantic basin.

In the next two years, two more NASA scatterometers are expected to be launched. The QuikSCAT will be launched in November 1998 to provide a "quick" fill of the lost time between the NSCAT and SeaWinds (early 2000 launch). The QuikSCAT is built from SeaWinds spare parts and will return a 1,800 km wide wind swath that will enable it to cover

52

90% of the ocean surface each day. The later SeaWinds instrument will have the same capabilities and have an expected operational lifetime of three years. The techniques proposed in this thesis should be further validated to gain a better understanding of TC structure and provide critical wind radii inside the radius for which accurate scatterometer winds may be obtained.

REFERENCES

Carr, L. E., and R. L. Elsberry, 1994: Systematic and integrated approach to tropical cyclone track forecasting. Part I. Approach overview and description of meteorological basis. Tech. Rep. NPS-MR-94-002, Naval Postgraduate School, Monterey, CA, 273 pp.

Carr, L. E., and R. L. Elsberry, 1997: Models of tropical cyclone wind distribution and beta-effect propagation for application to tropical cyclone track forecasting. *Mon. Wea. Rev.*, **125**, 3190-3209.

Fisher, M. R., 1996: Western North Pacific tropical cyclone wind structure and structure changes. Masters thesis, Naval Postgraduate School, Monterey, CA, 53 pp.

Holland, G. J., 1980: An analytical model of the wind and pressure profiles in hurricanes. *Mon. Wea. Rev.*, **108**, 1212-1218.

Merrill, R. T., 1984: A comparison of large and small tropical cyclones. *Mon. Wea. Rev.*, **112**, 1408-1418.

Naderi, F. M., M. H. Freilich, and D. G. Long, 1991: Spaceborne radar measurement of wind velocity over the ocean - an overview of the NSCAT scatterometer system. *Proc. IEEE*, **79**, 850-866.

Riehl, H., 1963: Some relations between wind and thermal structure of steady state hurricanes. *J. Atmos. Sci.*, **20**, 276-284.

Schloemer, R. W., 1954: Analysis and synthesis of hurricane wind profiles over Lake Okechobee, FL. Hydromet Rep. 31, 49 pp. [Govt. Printing Office, No. C30.70:31].

Weatherford, C. L., and W. M. Gray, 1988a: Typhoon structure as revealed by aircraft reconnaissance. Part I: Data analysis and climatology. *Mon. Wea. Rev.*, **116**, 1032-1043.

_____, and _____, 1988b: Typhoon structure as revealed by aircraft reconnaissance. Part II: Structural variability. *Mon. Wea. Rev.*, **116**, 1044-1056.

INITIAL DISTRIBUTION LIST

No. Copies

1. Defense Technical Information Center 2
   8725 John J. Kingman Rd., STE 0944
   Ft. Belvoir, VA 22060-6218

2. Dudley Knox Library 2
   Naval Postgraduate School
   411 Dyer Rd.
   Monterey, CA 93943-5101

3. Meteorology Department 1
   Code MR/Wx
   Naval Postgraduate School
   589 Dyer Rd Rm 254
   Monterey CA 93943-5114

4. Oceanography Department 1
   Code OC/BO
   Naval Postgraduate School
   833 Dyer Rd Rm 331
   Monterey CA 93943-5122

5. Dr. R. L. Elsberry 2
   Code MR/Es
   Naval Postgraduate School
   589 Dyer Rd Rm 254
   Monterey CA 93943-5114

6. Dr. L. E. Carr III 1
   Code MR/Cr
   Naval Postgraduate School
   589 Dyer Rd Rm 254
   Monterey CA 93943-5114

7. Capt Scott G. Magnan 1
   3410 Henery Rd
   Bellevue NE 68123

8. Commanding Officer   1
   Fleet Numerical Meteorology and Oceanography Center
   7 Grace Hopper Ave Stop 4
   Monterey CA 93943-0120

9. Chief of Naval Research   1
   800 N. Quincy Street
   Arlington VA 22217

10. Air Force Institute of Technology/CIG BLDG 125   1
    2950 P Street
    Wright-Patterson AFB OH 45433-7765

11. Commanding Officer   1
    Naval Pacific Meteorology and Oceanography Center
    NAVPACMETOCEANCEN Box 113
    Pearl Harbor, HI 96860-5050

12. Commanding Officer   1
    Naval Pacific Meteorology and Oceanography Center
    COMNAVMARIANAS Box 12
    FPO AP 96540-0051